AD_____

Award Number:

W81XWH-11-2-0218

TITLE:
Identification of New Drug Targets in Multi-Drug Resistant Bacterial Infections

PRINCIPAL INVESTIGATOR:

Andrew M. Gulick, PhD

CONTRACTING ORGANIZATION:
Hauptman-Woodward Medical Research Institute
Buffalo NY 14203

REPORT DATE:

October 2013

TYPE OF REPORT:

Annual

PREPARED FOR: U.S. Army Medical Research and Materiel Command
Fort Detrick, Maryland 21702-5012

DISTRIBUTION STATEMENT:

☑ Approved for public release; distribution unlimited

# REPORT DOCUMENTATION PAGE

*Form Approved*
*OMB No. 0704-0188*



| 1. REPORT DATE | 2. REPORT TYPE | 3. DATES COVERED |
|---|---|---|
| October 2013 | Annual | 26September2012–25September2013 |

**4. TITLE AND SUBTITLE**
Identification of New Drug Targets in Multi-Drug Resistant Bacterial Infections

**5a. CONTRACT NUMBER**
W81XWH-11-2-0218

**5b. GRANT NUMBER**
W81XWH-11-2-0218

**5c. PROGRAM ELEMENT NUMBER**

**6. AUTHOR(S)**
Andrew M. Gulick, Ph.D., Thomas A. Russo, MD, CM, L. Wayne Schultz, Ph.D., Timothy C. Umland, Ph.D.

E-Mail: gulick@hwi.buffalo.edu

**5d. PROJECT NUMBER**

**5e. TASK NUMBER**

**5f. WORK UNIT NUMBER**

**7. PERFORMING ORGANIZATION NAME(S) AND ADDRESS(ES)**

Hauptman Woodward Medical Research Institute, Inc.
Buffalo, NY 14203-1102

The Research Foundation for SUNY on behalf of University at Buffalo
Buffalo, NY 14260-7016

**8. PERFORMING ORGANIZATION REPORT NUMBER**

**9. SPONSORING / MONITORING AGENCY NAME(S) AND ADDRESS(ES)**
U.S. Army Medical Research and Materiel Command
Fort Detrick, Maryland 21702-5012

**10. SPONSOR/MONITOR'S ACRONYM(S)**

**11. SPONSOR/MONITOR'S REPORT NUMBER(S)**

**12. DISTRIBUTION / AVAILABILITY STATEMENT**
Approved for Public Release; Distribution Unlimited

**13. SUPPLEMENTARY NOTES**

**14. ABSTRACT**

**Progress Report**: We are combining two parallel efforts to explore new targets and pathways in A. baumannii. We hypothesize that two proteins involved in aromatic amino acid and metabolite biosynthesis are essential and are valid targets for development of inhibitors as potential antibiotics. We additionally hypothesize that a novel natural product is produced by A. baumannii that may play a role in pathogenesis or virulence.
Goal 1. We aim to validate two protein targets that have been identified through genetic screening as essential targets in *A. baumannii*. These targets will be biochemically and structurally characterized, and will be screened in silico for potential fragment-based ligands that could bind to the enzyme active site. Conservation and prevalence of the targeted genes for goal 1 confirm essentiality and cloning, expression, purification, and preliminary crystallization was completed during year 1. Goal 2. We will characterize biochemically a novel natural product biosynthetic pathway to identify a new secondary metabolite and characterize the phenotype of a deletion strain that is unable to produce this compound. All genes for goal 2 have been cloned and catalytic proteins have been purified. Functional reconstitution of this pathway was initiated, identifying potential natural product building blocks. A structure of one protein has been determined.

**15. SUBJECT TERMS**
Acinetobacter baumannii, structural biology, genetic screening, biosynthetic pathways, essential gene identifcation

| 16. SECURITY CLASSIFICATION OF: | | | 17. LIMITATION OF ABSTRACT | 18. NUMBER OF PAGES | 19a. NAME OF RESPONSIBLE PERSON |
|---|---|---|---|---|---|
| a. REPORT | b. ABSTRACT | c. THIS PAGE | | | 19b. TELEPHONE NUMBER *(include area code)* |
| U | U | U | UU | 36 | USAMRMC |

# Table of Contents

## Introduction

*A. baumannii* is a gram-negative bacillus (GNB) known to cause health-care associated infections. Recently, community-acquired infections, infections in wounded U.S. service members, and infections in residents of long-term care facilities have been reported. The incidence of Acinetobacter infection in all venues is increasing worldwide. The changing epidemiology and incidence of infections due to Acinetobacter establishes it as a pathogen of increasing medical importance. Further, *A. baumannii* has acquired an alarming number of antimicrobial resistance genes. Resistance to all aminoglycosides, cephalosporins, and fluoroquinolones is common and resistance to carbapenems and beta-lactamase inhibitors is increasing. Safe reliable agents with predictable activity against *A. baumannii* are presently non-existent. Improved outcomes will require the development of new therapeutics. We aim to accomplish this is by identifying and examining two biosynthetic pathways as potential antimicrobial targets in *A. baumannii*. Our investigation of protein targets in *A. baumannii* includes two goals. The **first goal** focuses on validating chorismate synthase (CS) and prephenate dehydrogenase/3-phosphoshikimate-1-carboxyvinyl transferase (PD-PSCVT) as therapeutic targets in the *A. baumannii*. We will experimentally establish the prevalence and *in vivo* essentiality of these genes in multiple strains of *A. baumannii*. We will recombinantly express, purify, assay, and structurally characterize the CS and PD-PSCVT enzymes. Finally, we will evaluate the druggability of these proteins through structural and computational methods. The **second goal** will continue our efforts to characterize the natural product biosynthetic machinery of pathogenic GNB. We will examine a novel biosynthetic cluster that encodes non-ribosomal peptide synthetase (NRPS) enzymes that have been demonstrated to be involved in bacterial motility and to be upregulated in response to quorum signaling molecules. We will assay the synthetic enzymes to identify the substrate building blocks, identify the natural product through *in vitro* reconstitution and analysis of mutant strains, and assay the role of this pathway in bacterial growth and virulence.

# Body

### Goal 1. Validation of Chorismate Biosynthesis as an Essential Target of *A. baumannii*

Our group has developed a novel and efficient approach to identify GNB genes and their protein products that are essential for growth and/or survival during infection, which is then validated via a rat soft-tissue infection model (*1*). This method has established that chorismate synthase (CS) and the bifunctional prephenate dehydrogenase 3-phosphoshikimate-1-carboxyvinyl transferase (PD-PSCVT) are essential proteins for *A. baumannii* infection (Figure 1) (*2*). Furthermore, PSCVT is a proven druggable target in plants (*3*), and the chorismate pathway is absent in humans. Therefore, our hypothesis is that these proteins are potential therapeutic targets in GNB. The object of this goal is to validate these proteins in the chorismate biosynthesis pathway as therapeutic targets.

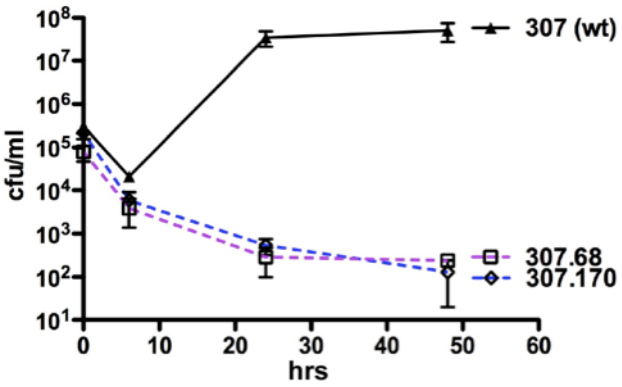


**Figure 1.** The mutant derivatives of the *A. baumannii* wild-type strain AB307-0294, AB307.68 and AB307.170, undergo significant and durable kill in the rat soft tissue infection model. AB307-0294 (wild-type), AB307.68 (*pd-pscvt*-minus), and AB307.170 (*cs*-minus). Data are Mean ± S.E.M. for n=3-4 for each time point.

PD-PSCVT and CS are part of the chorismate biosynthetic pathway, which is critical for the synthesis of the folate cofactors, bacterial siderophores, and aromatic amino acids (Figure 2). These enzymes from *A. baumannii* have not been studied. Moreover, inactivation of multiple enzymes within this pathway will decrease the likelihood of the development of resistance, as was done with trimethoprim-sulfamethoxazole for the folate biosynthesis pathway. A similar metabolic pathway is present in other GNB exhibiting increasing occurrences of drug resistance (e.g., *Pseudomonas aeruginosa*, *Escherichia coli*, Enterobacter species, and *Klebsiella pneumoniae*), and our studies may translate to other GNB.

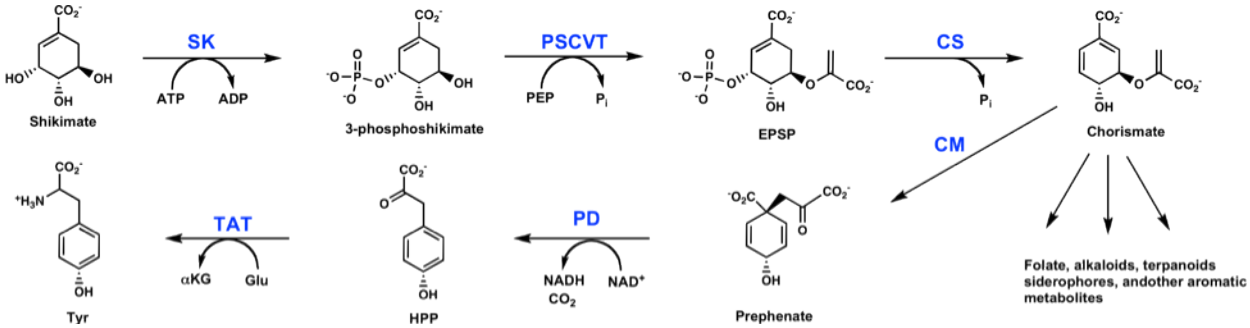


**Figure 2. Chorismate biosynthesis**. The biochemical steps in the synthesis of chorismate and tyrosine are shown to illustrate the enzymatic activities targeted in Goal 1. The PSCVT activity of PD-PSCVT couples 3-phosphoshikimate with pyruvate to produce 5-enoylpyruvyl-shikimate-3-phosphate (EPSP). Chorismate synthase (CS) is a lyase that removes the 3-phosphate to produce chorismate, a key building block for the formation of many aromatic compounds. The PD of PD-PSCVT removes a hydride from prephenate to form the aromatized product hydroxyphenylpyruvate (HPP), which then serves as the substrate for tyrosine aminotransferase (TAT), the enzyme that catalyzes the final step in tyrosine synthesis.

***Prevalence and conservation studies of CS and PD-PSCVT.*** An important consideration in validating a gene as an antimicrobial target is its level of conservation across strains. We have performed both a bioinformatic analysis and experimental verification of *cs* and *pd-pscvt* gene prevalence and sequence conservation. Thus far we have not observed any strains lacking either gene or displaying significant sequence variations (i.e., for *cs*: ≥99% identical at the nucleotide level, 100% identical at the amino acid level; for *pd-pscvt*: ≥98% identical at the nucleotide level, ≥99% identical at the amino acid level), supporting our hypothesis that these two genes are essential *in vivo* in numerous *A. baumannii* strains. Perhaps the most significant difference observed was in the PD-PSCVT protein, which exhibited differences in length due to a truncation/extension at the N-terminus, however, the active sites remain highly conserved. The *A. baumannii* strains formed two groups having either 748 or 756 amino acid residues in PD-PSCVT. It is unknown if this N-terminal truncation/extension has any functional significance. Table 1 summarizes the strains considered, including the geographical origin of each isolate, the occurrence of a multi-drug resistance (MDR) phenotype, and the tissue or body fluid the strain was isolated from, if known. The genomes of the majority of the strains have been both completely sequenced and annotated, or this process is currently underway. Three additional strains (AB932, AB1013, and ATCC 15308) lacking significant genomic sequence data are also under consideration, as two represent military isolates and the third has been a strain widely distributed for laboratory studies. For these strains, the respective genes were amplified by PCR from genomic DNA templates and then sequenced. A second related important consideration in the selection of antimicrobial targets is the determination of the lack of additional genes capable of overlapping function but potentially possessing sequence differences that may manifest themselves as a drug resistance mechanism. Thus far we have not identified the presence of any potential paralogous *cs* or *pd-pscvt* genes in any of the analyzed strains. While not conclusive, this observation suggests the absence of a related parallel biosynthetic pathway in *A. baumannii*.

Table 1. *A. baumannii* strains

| Strain | Origin (Isolated/Sequenced) | Notes‡ |
|---|---|---|
| 1656-2 | Kyungpook National University | MDR hospital isolate, South Korea |
| AB0057 | WRAMC / Case Western Reserve Univ. | MDR bloodstream isolate from WRAMC (military) |
| AB307-0294 | SUNY-Buffalo | Bloodstream isolate, ECMC, Buffalo |
| ACICU | Hospital S. Giovanni-Addolorata, Rome, Italy | MDR Hospital strain from an outbreak in Rome; cerebrospinal fluid isolate |
| ATCC 17978 | ATCC | Clinical isolate, fatal meningitis (1951) |
| AYE | Le Kremlin-Bicêtre, France | Clinical isolate, pneumonia and a urinary tract infection |
| MDR-ZJ06 | Zhejiang University, China | MDR bloodstream isolate, Hangzhou, China |
| SDF | Marseille, France | Isolated from body lice in France; presumably result of lice feeding on blood of infected human |
| TCDC-AB0715 | Taipei, Taiwan | MDR clinical isolate, bloodstream |
| 6013113 | Birmingham, UK | Skin isolate, Human Microbiome Project reference strain |
| 6013150 | Birmingham, UK | Skin isolate, Human Microbiome Project reference strain |
| 6014059 | Birmingham, UK | Skin isolate, Human Microbiome Project reference strain |
| AB056 | WRAMC / Case Western Reserve Univ. | MDR bloodstream isolate from WRAMC (military) |
| AB058 | WRAMC / Case Western Reserve Univ. | MDR skin survey isolate from WRAMC (military) |
| AB059 | WRAMC / Case Western Reserve Univ. | MDR urine isolate from WRAMC (military) |
| AB900 | WRAMC / SUNY-Buffalo | Perineal isolate from WRAMC (military); obtained from Col. Craft |
| ATCC 19606 | ATCC | Urine isolate (originally Schaub's strain 81) |
| AB932 | WRAMC | Environmental isolate (military); obtained from Col. Craft |
| AB1013 | WRAMC | Environmental isolate (military); obtained from Col. Craft |
| ATCC 15308 | ATCC | Urine (originally named Schaub's strain Biol. 1) |

‡MDR: multi-drug resistant strain; WRAMC: Walter Reed National Military Medical Center
**Yellow**: Publically released completed genomes (http://www.ncbi.nlm.nih.gov/genomes/lproks.cgi).
**Green**: Genomic sequencing in Whole Genome Shotgun (WGS) assembly stage (http://gelportal.gel.ym.edu.tw/services/genomes/microb3.php).

***Establishing the in vivo essentiality of CS and PD-PSCVT in multiple strains of A. baumannii.*** CS and PD-PSCVT were identified in an initial screen for *in vivo* essentiality. Mutations in either gene in *A. baumannii* strain AB307-0294 compromise *A. baumannii* viability in the rat soft tissue infection model (*2*). We are now testing if CS and PD-PSCVT are *in vivo* essential across a library of *A. baumannii* strains in order to provide confidence that this is a general feature of *A. baumannii* and not a strain-specific phenotype.

Directed knockouts of each gene remain underway. We are having some success with a conjugative approach and therefore using it exclusively at this point. In this approach the construct is introduced into the *A. baumannii* background on a suicide plasmid via conjugation. In this manner, the DNA construct is introduced into *A. baumannii* in a highly efficient manner with the hopes of overcoming DNA restriction related degradation and poor efficiencies in site-specific recombination.

*E. coli* strains, CC118, SM10, and CC118/pKNG101 (pKNG101 is a 6.8kb suicide plasmid, *sacB*$^{+}$, R6K origin, Sm$^{r}$ ) were a generous gift from Dr. Phil Rather, Emory University. The AB932*aroC::kan::aroC* DNA fragment was cloned into pKNG101 resulting in the new plasmid pKNG∆*aroC*. Approximately 1kb of upstream and downstream sequence is included in this construct. This plasmid was maintained in the *E. coli* strain CC118.

The following protocol is presently being employed:

1- pKNG307*aroC::kan* has been electroporated into the *E.coli* strain SM10 for mating with *A. baumannii* strains.

2- The mating was done as follows: SM10/ pKNG307*aroC::kan* and the *A. baumannii* strain in question each were grown overnight in 3ml of LB broth with appropriate antibiotics added. In the morning, 500µL of each culture were centrifuged and the pellet was washed 3x with LB broth to eliminate antibiotics.

3-100µl of each culture were pre-mixed, centrifuged, resuspended in 100µL and plated onto a very dry LB plate.

4- The mating mixture was incubated at 37°C for 7 hours.

5- A suspension of the mates was made in 4mL of LB medium, serially diluted and plated on LB plates containing nitrofurantoin (5µg/mL) to counter-select against the *E.coli* SM10 strain and streptomycin (50µg/mL) and kanamycin (40µg/mL) to select for integration of pKNG307*aroC::kan* into the AB chromosome.

6- Transconjugants were purified on LB-nitrofurantoin (5µg/mL)-streptomycin (50µg/mL) and kanamycin (40µg/mL) plates to confirm they possess the correct genetic markers.

7- Transconjugants that possess the correct resistance markers were plated onto LB-sucrose (10%)-kanamycin (40µg/mL) plates and incubated at room temperature for 48 hours. This step takes advantage of *sacB* being present on pKNG101. Colonies that grow on the sucrose plate will have had the pKNG101 plasmid cured. This is the desired construct in which *aroC* has been disrupted and the delivery plasmid has been lost.

Using this modified protocol, we have been able to generate site-specific constructs in 3 *A. baumannii* strains with successful "cure" of pKNG101; AB307-0294, AB714, and AB764. This is exciting because the later 2 strains are the first two non-AB307-0294 strains in which it appears that *aroC* has been successfully disrupted. Sequence analysis studies confirmed the successful disruption of *aroC* (data not shown).

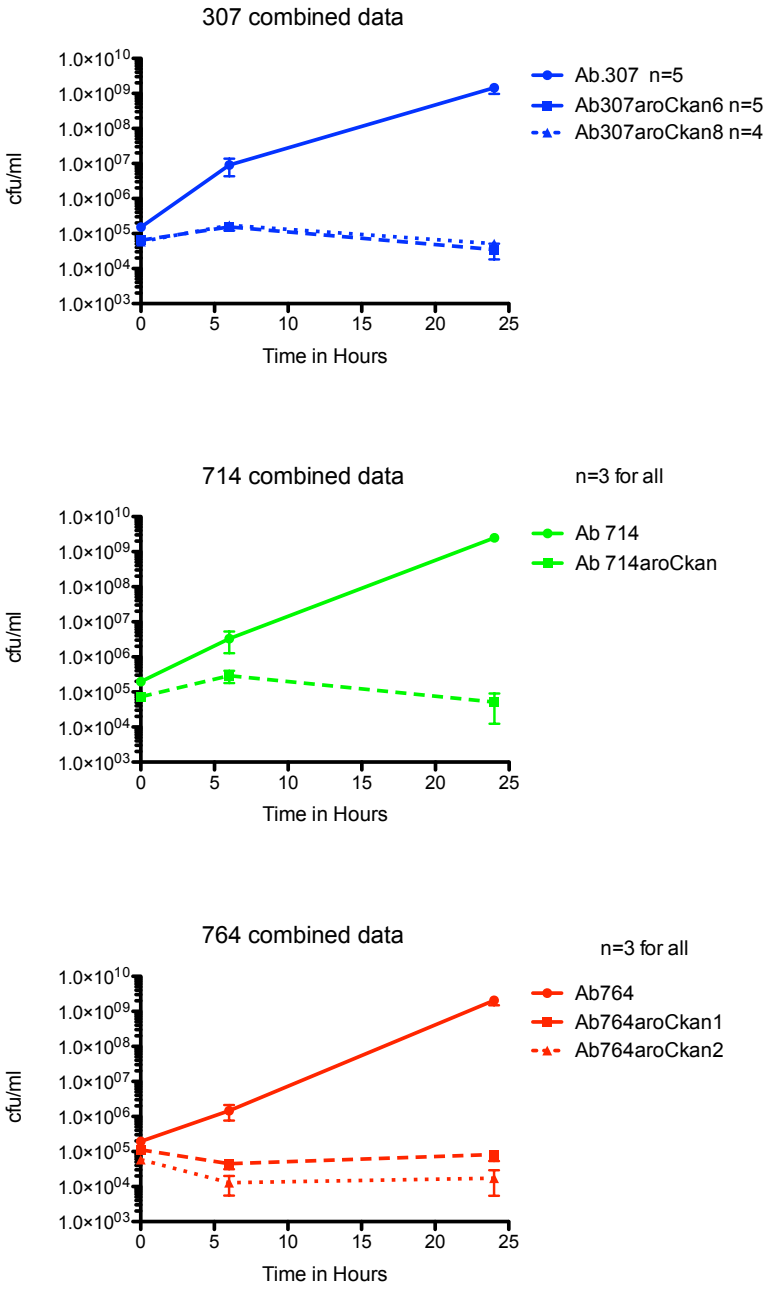


**Figure 3**. Growth curves of aroC knockouts.

Ex vivo biologic analysis of AB714Δ*aroC* and AB764Δ*aroC*.

In human ascites, the phenotype of AB307-0294Δ*aroC* was an inability to grow. As a first step, we assessed the growth of AB714Δ*aroC* and AB764Δ*aroC* in human ascites ex vivo.

The data depicted in Figure 3 demonstrate that disruption of *aroC* ex vivo in AB714 (AB714Δ*aroC)* and AB764 (AB764Δ*aroC)* results in the same phenotype as (AB307-0294Δ*aroC).* These data demonstrate, at least for these 3 strains, that no alternative biosynthetic pathway exists and therefore *aroC* is essential, at least ex vivo. As a next step in vivo studies are being planned.

In vivo biologic analysis of AB714Δ*aroC* and AB764Δ*aroC*.

The next step was an in vivo assessment of AB714, AB764 and their derivatives with a disruption in *aroC* (AB714Δ*aroC* and AB764Δ*aroC* respectively). The University at Buffalo and Veterans Administration Institutional Animal Care Committees approved the rat subcutaneous abscess model. This study was carried out in strict accordance with the recommendations in the Guide for the Care and Use of Laboratory Animals of the National Institutes of Health and all efforts were made to minimize suffering. Briefly, a subcutaneous space is created through the injection of 30 ml of air into the back of anesthetized Long-Evans rats (200-225 grams), followed by the injection of 1 ml of 1% croton oil in a filter-sterilized vegetable oil vehicle. The space was

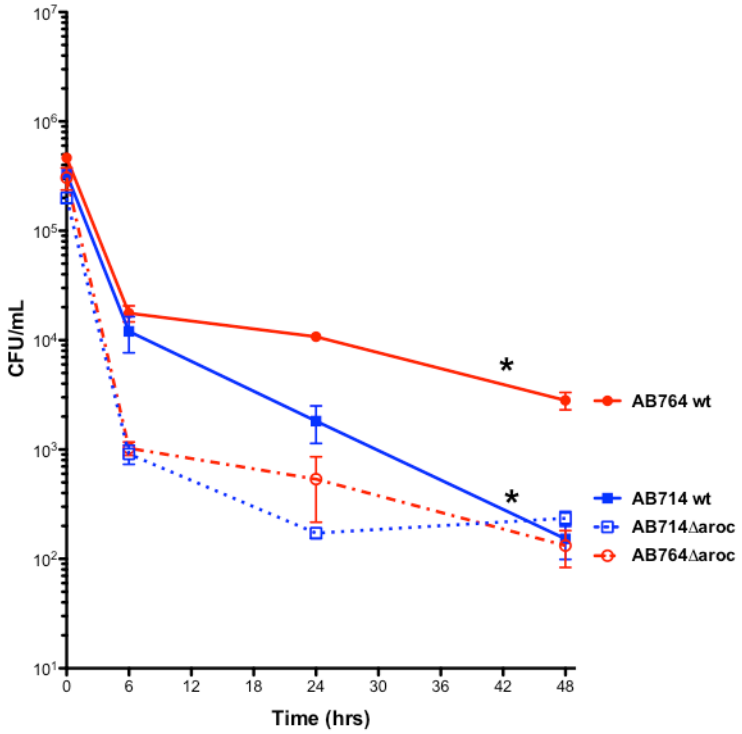


**Figure 4.** Growth curves for *Ex vivo* biologic analysis of AB714Δ*aroC* and AB764Δ*aroC.*

allowed to mature into an encapsulated, fluid-filled (8-12 ml) "pouch" over 6-8 days. Neutrophils would have migrated into the abscess in response to appropriate chemotactic signals. The abscess' subcutaneous location enabled multiple injections and samplings to be performed over time. AB714, AB714Δ*aroC*, AB764, and AB764Δ*aroC* were injected alone into the abscess of an anesthetized animal, resulting in estimated starting abscess concentration of 2-4 x $10^5$ CFU/mL. Within one minute after the bacteria were injected into the abscess 0.5 mL of abscess fluid was removed to measure the actual starting bacterial titer. Fluid aliquots (0.5 mL) were subsequently obtained from anesthetized animals 6, 24, and 48 hours after the initial bacterial challenge and bacterial titers enumerated. *In vivo* data are presented as mean ± SEM. To normalize *in vivo* data $\log_{10}$ transformed values were utilized, the area under each curve was calculated, and these areas compared using two-tailed unpaired t tests (Prism 4 for Macintosh, GraphPad Software Inc.).

In this experiment (Figure 4), the AUC, which reflects overall growth/survival was significantly greater for AB714 compared to AB714Δ*aroC* (P = 0.011) and for AB764 compared to AB764Δ*aroC* (P= 0.0028). However, the growth/survival of these wild-type strains was not as great as anticipated nor as previously observed for AB307-0294, which grows and achieves a plateau density of >$10^8$ CFU/mL. Therefore, the experimental conditions were not optimal to observe maximal differences between strain pairs. Nonetheless, observed differences were as expected.

In summary, *aroC* has been successfully disrupted as designed in AB307-0292, AB714 and AB764 and the phenotypes are as predicted. We may repeat studies with AB714, AB764 and their *aroC* mutant derivatives in the rat subcutaneous infection model using higher starting titers (approximately 1 x $10^7$ CFU/mL) if time and resources permit. Studies to disrupt *aroA* in these strains are underway.

**Shikimate Kinase, a new drug target**

Shikimate kinase (SK) catalyzes the phosphorylation of the 3'-hydroxyl of shikimate to form shikimate 3-phosphate (S3P), the substrate for PSCVT. As part of this project, we cloned, expressed and purified SK in order to biosynthesize S3P, an expensive reagent needed to assess the activity of PSCVT. However, we realized that SK represented a possible drug target by itself. Recent work has focused on SK as a target for *Mycobacterium tuberculosis* (*4*), but

there has been little attention to GNB like *A. baumannii*. Some GNB, such as E. coli, have two genes with SK activity, thereby reducing interest in a target that has redundant activity. *A. baumannii*, like *M. tuberculosis*, has only one gene producing SK activity and therefore would likely be sensitive to SK inhibitors. As a first step to investigating SK as target, we crystallized and determined the structure of SK in complex with the substrate shikimate.

**Figure 5**. Crystals of shikimate kinase. Although the crystals have bipyramidal morphology, diffraction experiments indicate that the internal structure is orthorhombic.

Crystals of SK were produced from 1.5M sodium/potassium phosphate pH 6.9, appear after 3 days and grow to sizes of 0.5 x 0.5 x 0.5mm$^3$ (Figure 5). The structure of AB shikimate kinase (SK) was solved and refined to a resolution of 2.1Å. Refinement data statistics are reported in Table 2.

The overall structure is similar to other bacterial shikimate kinases and contains a shikimic acid molecule bound in the active site (Figure 6A). The electron density was defined for the full protein chain and very clear for the shikimic acid (Figure 6B). The shikimic acid is held in place by arginine and glutamic acid residues from opposite sides of the structure. This arrangement likely serves to stabilize the overall protein

**Table 2. Shikimate Kinase X-ray Data and Refinement Statistics**

| **Data Statistics** | **Shikimate Kinase** |
|---|---|
| Wavelength (Å) | 1.54 |
| Space group | $I2_12_12_1$ |
| Cell dimension | |
| a, b, c (Å) | 80.60, 85.18, 115.8 |
| α, β, γ (°) | 90, 90, 90 |
| Molecules/asymmetric unit | 1 |
| Resolution range (Å)* | 50-2.1 (2.14-2.10) |
| No. of observations | 368,852 |
| No .of unique reflections | 23,342 |
| I/σ(I)* | 56.2 (5.6) |
| Data Completeness (%)* | 98.4 (97.6) |
| $R_{merge}$* | 0.056 (.333) |
| Overall Wilson B-factor | 43.5 |
| $R_{work}$ | 0.19 (0.23) |
| $R_{free}$ | 0.22 (0.32) |

*Numbers in parentheses refer to statistics for the highest resolution data shell.

structure offering a reasonable explanation for poor crystal quality found when shikimic acid is not included in the crystallization experiment. Although ADP was included in the crystallization, we do not see it bound in the active site. Instead, there is a phosphate ion (from the crystallization cocktail) occupying the position normally held by the terminal ADP phosphate. At first review, the protein has multiple sites that might be targeted by drug molecules. Our approach will be to screen drug fragment libraries to look for ligands that bind at or near the shikimate binding site. As described below, we have developed both a biochemical assay and a differential scanning fluorimetry assay to screen drug libraries. With the structure in hand, *in silico* screening for ligands can be initiated.

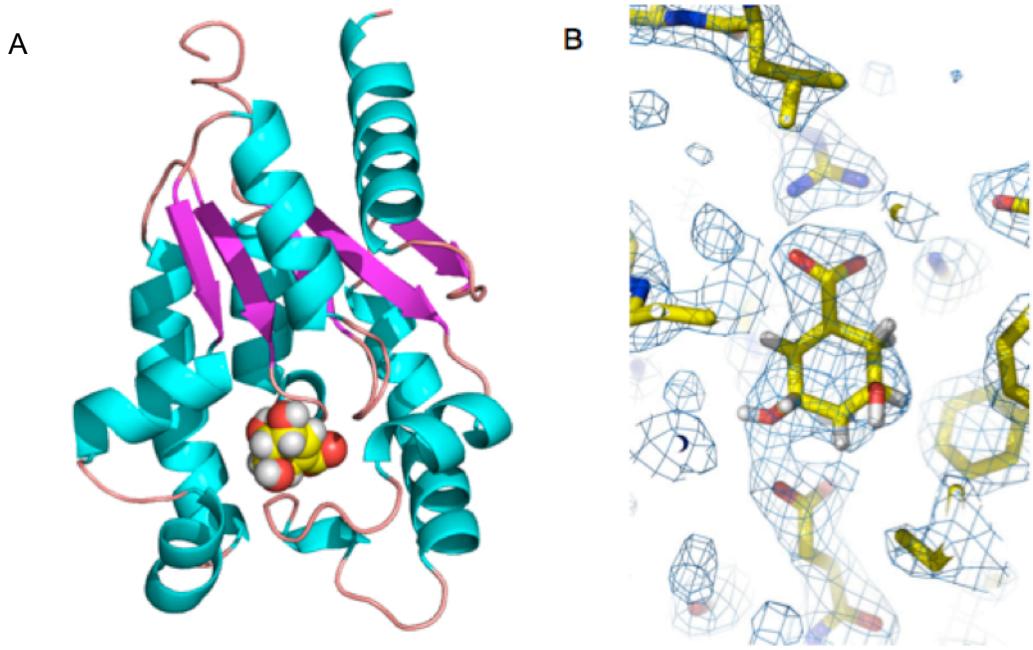


**Figure 6.** The structure of *Acinetobacter baumannii* shikimate kinase (AbSK). **A.** A ribbon diagram representing the overall structure and fold of AbSK. Shikimic acid, the substrate (yellow) is bound in the active site. **B.** The electron density map shows clearly the position and conformation of shikimic acid in the active site.

**PSCVT structural studies**

In the past year, we solved the structure of the individual PSCVT domain. We had decided to pursue the crystallization of the individual PSCVT domain from the PD-PSCVT protein as a solution to the poor crystals formed by the full-length fusion protein. After a difficult purification process involving 4 different chromatographic columns, the purified PSCVT yielded crystals. There were about 20 different conditions that yielded crystals, 14 of which were further optimized using sitting drops. This screen produced two conditions that grew similar plate-like crystals, 0.1 M Bis-Tris pH 5.5, 0.2 M Sodium Chloride, 25% PEG 3350 and 0.1 M Bis-Tris pH 6.5, 0.2 M Magnesium Chloride hexahydrate, 25% PEG 3350 (Fig. 7, A and C). UV microscopy (280nm) confirmed that the crystals are composed of protein (Fig. 7, B and D). From optimized crystals, we solved and refined the structure of the individual PSCVT domain from AB. The structure of PSCVT was solved by molecular replacement using the PSCVT and S3P complex from coxiella burnetii (PDB ID: 3SLH) as the starting model (52.1% sequence identity). Refinement of the individual PSCVT domain has been completed. The details of the data

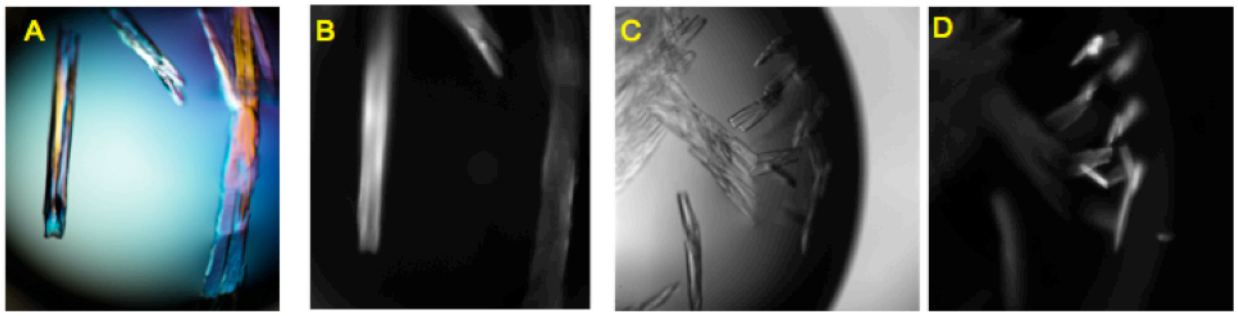


**Figure 7**. Crystals of the individual PSCVT domains from different crystallization conditions. Each crystallization experiment was recorded with visible (A and C) and UV light (B and D). The crystals (A and C) form from chemical conditions differing in pH and cations.

collection and refinement are shown in Figure 8. In previous work, PSCVT has been shown to occupy an open conformation in the absence of substrate (pdb2GG4) and more closed conformation when substrate is bound (pdb2AAY). Our structure is found to occupy a partially open conformation (Fig. 8). Even though the shikimate 3-phosphate (S3P) substrate was included in the crystallization, it did not appear to have significant occupancy in the active site and may explain why our structure is in a partially open conformation. For the purpose of drug screening, the open conformation is ideal because the active site available to bind candidate ligands. The resolution extends to 2.37 Å where it will be possible to see the conformation of bound ligands and inhibitors. With this structure in hand, we can begin our screening campaign to look for inhibitors of PSCVT activity.

| **Data Collection Statistics** | |
|---|---|
| Wavelength (Å) | 1.54 |
| Space group | $P2_12_12_1$ |
| Cell dimensions | |
| a, b, c (Å) | 73.893, 103.380, 113.204 |
| α, β, γ (°) | 90, 90, 90 |
| Molecules/asymmetric unit | 2 |
| Resolution range (Å) | 34.79-2.37 (2.41-2.37) |
| No. of observations | 261575 |
| No. of unique reflections | 34943 |
| I/sig(I) | 17.4 (4.7) |
| Data completeness | 96.9 (99) |
| $R_{merge}$ | 0.082 (0.418) |
| **Refinement Statistics** | |
| $R_{work}$ | 0.2129 |
| $R_{free}$ | 0.2891 |
| No. of residues | 884 |
| No. of waters | 69 |
| RMS bond length | 0.01 |
| RMS bond angle | 1.41 |

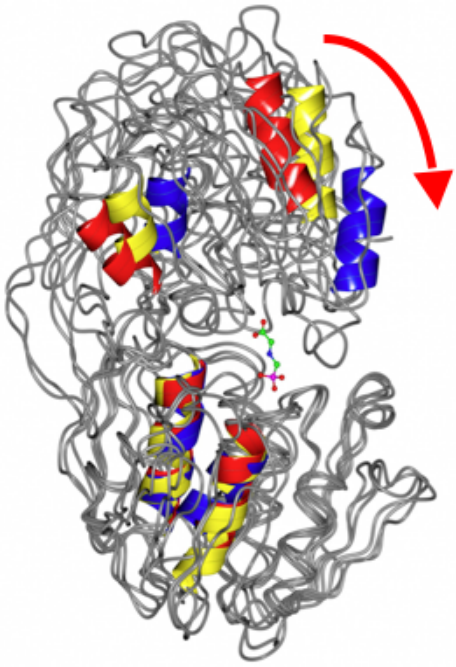

**Figure 8**. Table of X-ray data collection and refinement statistics. The structure of the individual domain of PSCVT is in the open conformation. Superposition of the N-terminus (residues 14-200) of the *A. baumannii* PSCVT (yellow) with PSCVT in the open conformation (red)(pdb2GG4) and the closed substrate bound conformation (blue)(pdb2AAY). The red arrow indicates the direction of motion upon closing.

**SK and PSCVT assays.** In the shikimate pathway, SK converts shikimate to shikimate 3-phosphate (S3P), which is fused with phosphoenolpyruvate by PSCVT to create enolpyruvyl-shikimate 3-phosphate (EPSP) and inorganic phosphate. Two separate assays were used to determine the activity of SK and PSCVT. Each assay was developed as a single point reporter for microplate based screening of inhibitors. The SK assay uses a coupled system to detect the formation of ADP during the reaction (*5*) (Fig. 9A). The PSCVT assay measures the change in color of a dye that is responsive to inorganic phosphate, a product of the reaction (*6*) (Fig. 9B). These relatively simple assays will allow for the rapid and high throughput screening of chemical libraries to search for compounds with inhibitory activity. The goal is to identify compounds that inhibit both SK and PSCVT, thereby identifying a single compound with two targets. A multi-target approach such as this can increase the effectiveness of an antibiotic but also reduce the development of resistance.

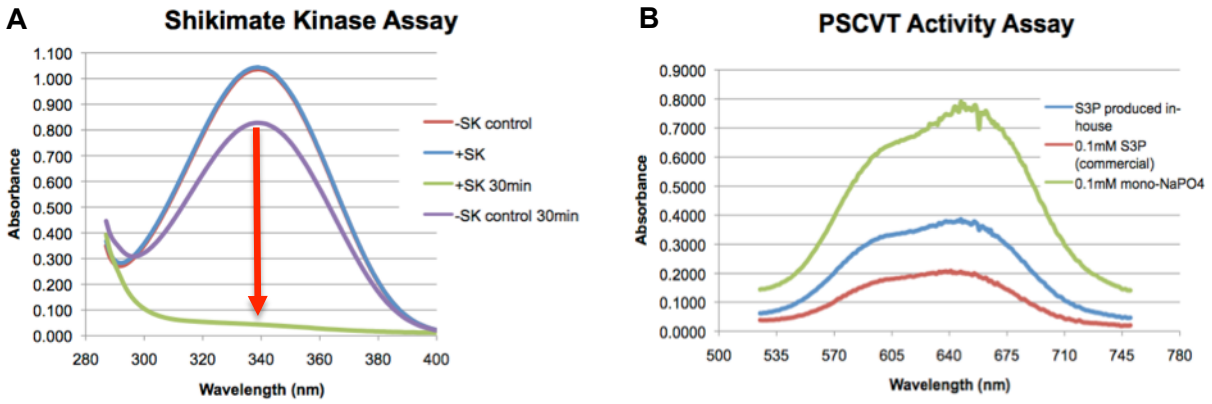


**Figure 9.** SK and PSCVT assays. **A.** The SK assay monitors the decrease in signal at 340nm that reports on the production of ADP from ATP by SK. The significant change in signal after 30 minutes reaction time (red arrow), provides enough sensitivity to screen for easy screening of inhibitors. **B.** The PSCVT assay monitors the increase in signal at 640nm that is created by a dye color change in response to inorganic phosphate production. Our in-house biosynthesized S3P (blue line) performs better than the commercial version (red line).

***Differential scanning fluorimetry (DSF)*** is a thermal-denaturation assay that measures the stability of a target protein and is used to measure the subsequent increase in protein melting temperature due to the binding of a ligand to the protein (*7*). The thermal unfolding is detected using a fluorescent dye that interacts with hydrophobic residues in the protein core. As the protein unfolds, more core residues are exposed and the fluorescence of the dye increases and reaches a plateau when the protein is completely unfolded. The change in fluorescence and temperature gradient are created and monitored in an RT-PCR instrument. The data can be plotted as fluorescence vs. temperature to define a curve for the thermal unfolding transition. DSF can be used to rapidly screen thousands of molecules for those that cause a shift in the melting point, indicating an interaction with the protein. We plan to use this method to screen a ligand fragment library of 500 compounds to find fragments that result in thermal melting point shifts for shikimate kinase (SK) and PSCVT. Once binding fragments are discovered, the structures of the protein:fragment complexes will be determined and serve as the starting points for structure based drug design. As an example of this technique, we used DSF to study the binding of shikimate to SK (Fig. 10). The thermal melting point of SK was increase by 5ºC in the presence of the shikimate substrate indicating that it will be possible to detect binding of fragments to SK.

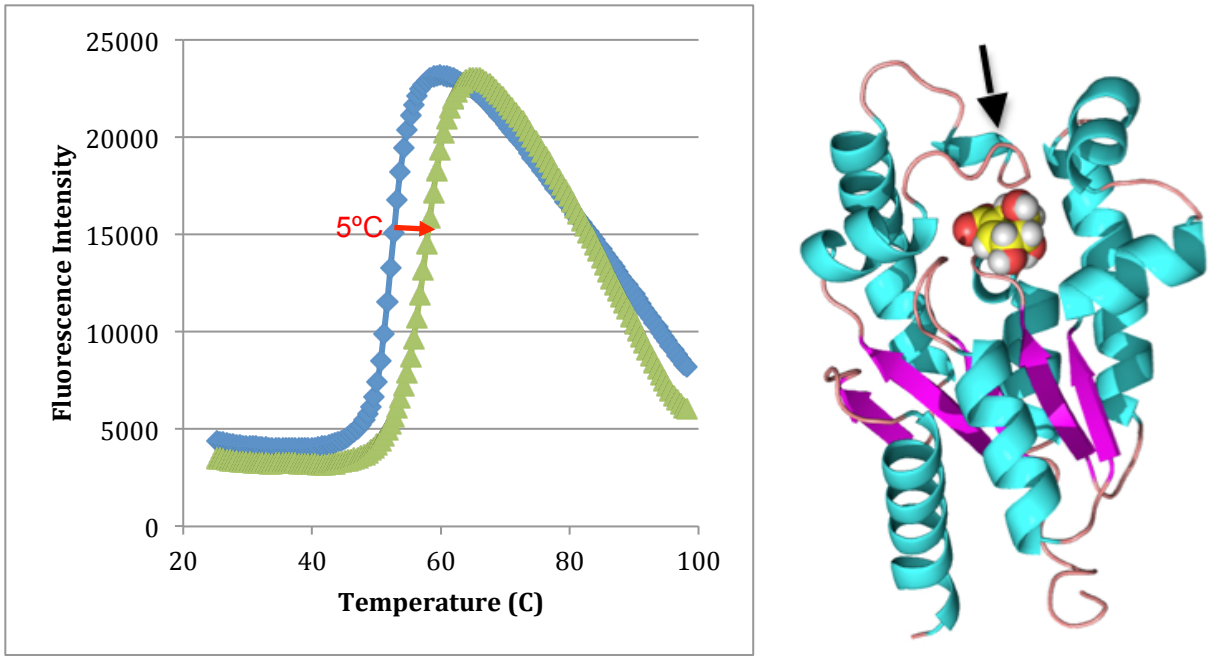


**Figure 10**. Differential scanning fluorimetry of shikimate kinase (SK). (Left) The melting temperature of SK increases when the substrate shikimate is added (shift of blue curve to green curve). The positive shift indicates that the ligand is stabilizing. (Right) The structure of SK with shikimate shows that the presence of the ligand stabilizes a lid structure that is disordered in the absence of ligand (black arrow).

### Chorismate Synthase

In Year 1 of this project, we reported crystallization conditions for Ab307 CS obtained from a crystallization screening protocol unique to HWI, employing 1536 conditions in a single microtitre plate. This screening protocol is samples 4x-16x more conditions within *crystallization space* than screens typically conducted elsewhere. Unfortunately these previous optimization attempts have thus far failed to provide diffraction-quality crystals. This prompted us to re-review our two initial 1536 condition crystallization screens, conducted at two different protein concentrations, to select previously overlooked conditions that differ significantly from those that have failed optimization. Specifically, we had been concentrating on conditions using polyethylene glycol (PEG) based crystallization cocktails, but crystallization reproducibility and crystal quality was poor, and significant protein precipitation accompanied crystallization. A sodium chloride (NaCl) based crystallization cocktail was selected and preliminary optimization was successfully performed. Figure 11 demonstrates the results of this preliminary optimization process. This optimization process first involved translation of the conditions identified from the 1536 screen, which was conducted using micro-batch under oil crystallization, to vapor diffusion crystallization. This was necessary to both scale up crystallization and to provide easier geometry for accessing crystals for soaking in ligands and mounting crystals for diffraction data collection. Following translation of the initial *hit* conditions, a systematic focused screening of similar conditions was conducted to improve crystallization.

The newly identified NaCl-based CS crystallization conditions then underwent optimization. During this optimization process, we observed that the crystallization window for Ab307 CS using NaCl as the crystallization agent is narrow. Furthermore, there is a strong correlation

between the pH and the NaCl concentration for the successful generation of CS single crystals. This pH-[NaCl] relationship is illustrated in Figure 12. For example, at a given NaCl concentration a change of pH by ≥ ±0.25 units can shift the results from obtaining well-formed single crystals to obtaining only precipitate or "micro-crystals". Likewise, for a given pH a change in NaCl concentration of ±0.2 M can have a similar influence on crystallization results. Additionally, the pH-[NaCl] crystallization window shifts as the pH changes, and visually the crystal quality is altered within the shifting crystallization window. Given the narrowness of the CS crystallization window, very fine screening about the initially identified successful crystallization conditions was necessary.

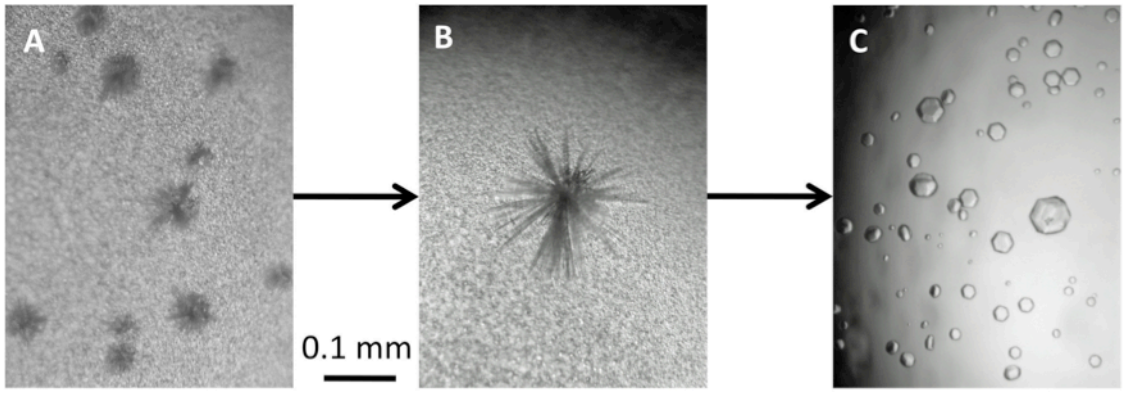


**Figure 11**. Initial optimization of CS crystallization using a NaCl based crystallization cocktail. (A) Results of translation of microbatch under oil crystallization conditions to hanging drop vapor diffusion crystallization yielded small clusters of poorly formed needle crystals. (B) Initial optimization yielded clusters of better-defined needle crystals. (C) Further optimization has resulting in the growth of single crystals with a hexagonal cross section.

Up to this stage of CS crystallization optimization, the outcomes of crystallization screening trials were judged solely on visual qualities of the results of the crystallization experiments (e.g., presence of precipitation, crystals, or the droplet remaining clear; size and morphology of crystals, etc.). The reason for evaluating the previously obtained crystals in this manner was because they were generally too small or poorly formed to serve as viable X-ray diffraction candidates. Now that conditions have been identified which yield larger crystals (~0.1 mm in the largest dimension), X-ray diffraction was employed to evaluate crystal quality. CS crystals were cryo-protected, flash-cooled in liquid nitrogen, and sent to the Stanford Synchrotron Radiation Lightsource (SSRL; mid-January 2013) for X-ray diffraction studies. Those crystals were representative of the crystals displayed in Figure 12 (~0.1 mm largest dimension). These crystals yielded only low-resolution (< 10 Å) diffraction data, and reliable determination of unit cell dimensions and the lattice symmetry was not possible. However, this initial diffraction test confirmed that the obtained crystals were protein and not salt crystals.

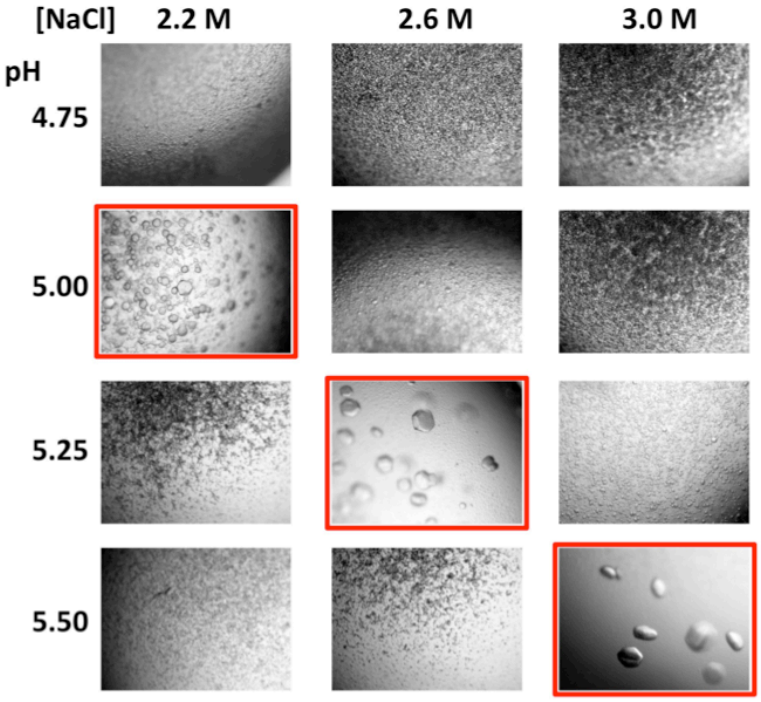


**Figure 12.** CS crystallization optimization. Microphotographs of hanging drop vapor diffusion crystallization experiments using a grid screen of NaCl concentration and pH equilibration reservoir conditions. These microphotographs were obtained approximately 1 week after setup of the crystallization experiments, and the largest crystals obtain were ~0.1 mm in the largest dimension. The red boxes indicate drops that contained well-formed crystals. The drop equilibrated against 2.2 M NaCl at pH 5.00 contained both small crystals and significant globular precipitate. The drops grown against 2.6 M NaCl at pH 5.25 and 3.0 M NaCl at pH 5.50, respectively, contained primarily crystals with minimal precipitate. However, the 2.6 M NaCl/pH 5.25 conditions resulted in smaller but better formed crystals than the 3.0 M NaCl/pH 5.50 conditions, indicating further fine screening was required.

Based on these initial diffraction test results, crystallization growth conditions were further optimized. These new crystallization conditions yielded a mixture of smaller crystals, similar to what was obtained under previous growth conditions, plus a small number of much larger and better-formed crystals (Figure 13).

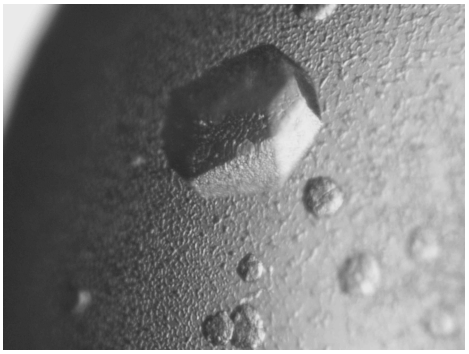

**Figure 13.** Example of a crystallization droplet containing both small (≤0.1 mm) crystals exhibiting poor morphology and a large well-formed (~0.35 mm) CS crystal.

These newly obtained crystals were then screened for diffraction at HWI's X-ray core facility. X-rays produced by HWI's lab source are several orders of magnitude less intense than those produced at a synchrotron lightsource, but diffraction data useful for characterizing crystals may still be obtained. A diffraction data set has been collected from one of these improved CS crystals, and preliminary analysis indicates that it is useful to 4-5 Å resolution. The diffraction data indicates that the crystals possess a hexagonal lattice with cell dimensions of $a$=$b$=87.1 Å, $c$=148.1 Å, with $\alpha$=$\beta$=90.0º and $\gamma$=120.0º. While further crystal improvement is required, this increased resolution obtained from a much weaker X-ray source was a highly positive indication that crystallization optimization was progressing.

CS crystallization optimization continued using X-ray diffraction as a key metric, using HWI's X-ray diffraction facility. First, various cryoprotectants were tested to determine if poor cryoprotection was the cause of the modest observed diffraction resolution. Diffraction data collection under cryo-conditions (~100K) is preferred as it minimizes radiation damage to the crystal. However, the process of adding cryoprotectants and flash-cooling protein crystals can result in damage to the crystal lattice (in non-technical terms, formation of micro or macro cracks). This, in turn, damages the quality of the diffraction data. The testing of different cryoprotection methods on the CS crystals has thus far not resulted in improved diffraction quality. CS crystals were then test for diffraction at room temperature, which does not require the addition of cryoprotectant and the subsequent flash cooling. This test demonstrated that the steps required for data collection under cryo-conditions were not the cause of the poor diffraction quality. Additionally, it demonstrated that the CS crystals were susceptible to radiation damage at room temperature, resulting in a complete loss of diffraction after only a short exposure. In an effort to improve the crystals, controlled dehydration of CS crystals via vapor diffusion was conducted. This dehydration method can result in a protein crystal lattice becoming more stable, as protein crystals typically contain a significant amount (e.g., 50%) of water by volume. Specifically, crystals in their mother liquor on a glass slide were transferred to fresh wells in a 24 well plate, with the wells containing higher concentrations of NaCl. These well-cover slip chambers were sealed with vacuum grease. After vapor diffusion equilibration between the crystal containing droplet and the well reservoir, the crystals were then tested for X-ray diffraction. The observed resolution did not significantly increase (~4-5 Å resolution maximum), but the diffraction spots were significantly sharper, indicating increased order within the crystal. See Figure 14. We are currently exploring this crystal dehydration strategy further as a strategy to improve crystal diffraction.

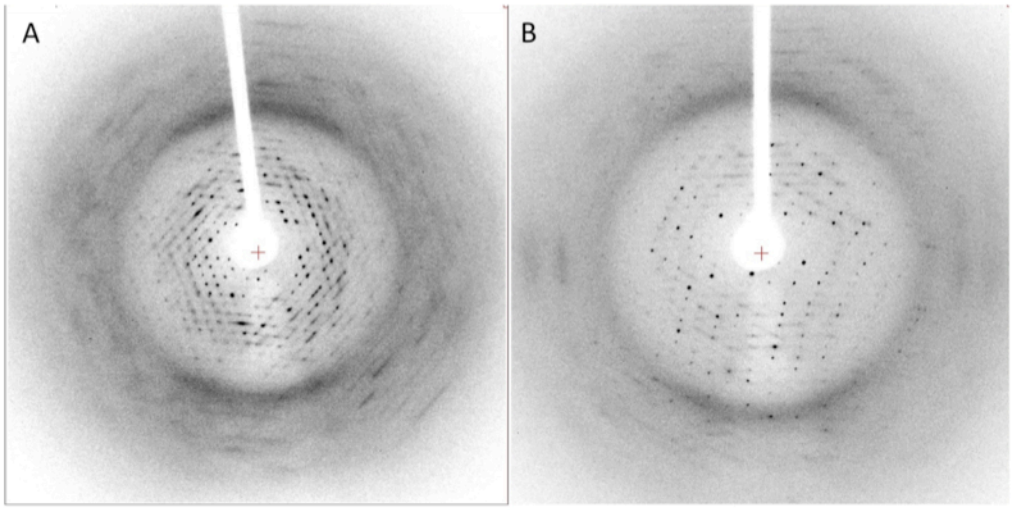


**Figure 14**. Examples of X-ray diffraction by CS crystals. A) An example of diffraction from a CS crystal tested at room temperature. Significant smearing of the diffraction spots is present, indicating internal disorder within the crystal. B) An example of diffraction from a CS crystal tested at room temperature following controlled dehydration of the crystal. The dehydration procedure sharpened the diffraction spots, indicating an improvement of internal crystal order.

In May-June, 2013, expression and purification of a new CS sample was completed to replenish depleted stocks. Most noteworthy, the CS purification protocol was improved to efficiently resolve the expected tetrameric form of CS from a larger molecular weight complex likely containing a misfolded or aggregated form of CS using ion exchange and then verified using gel filtration chromatography. Importantly, once these two CS species were resolved, the tetrameric

species remained stable (i.e., no observed conversion to the higher molecular weight species as a function of time). Crystallization was used to assay these two resolved CS oligomeric species, which migrate identically on SDS-PAGE at an estimated mass expected for the CS monomer. The tetrameric form readily crystallized whereas the larger molecular weight CS species failed to crystallize and generally resulted in heavy precipitation during crystallization screening. We determined that our previous CS preparations contained primarily the tetrameric form of CS but a modest amount of the higher molecular weight species was also present. The presence of this misfolded species likely inhibits the growth of high quality CS crystals.

Combining the more oligomeric homogeneous CS sample with the previously determined NaCl/citrate crystallization conditions yielded a new hexagonal morphology (Fig. 15A and B) and malonate based crystallization conditions yielded clusters of needle and thin plate crystals (Fig. 15C). These conditions underwent additional optimization.

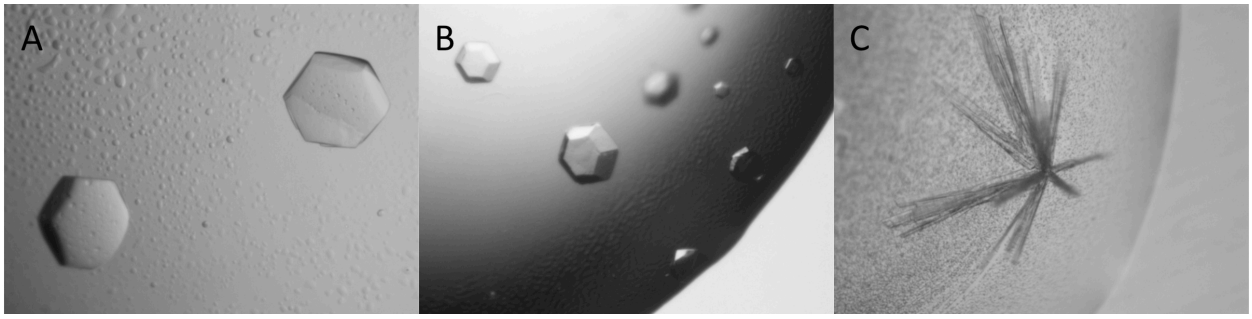


**Figure 15**. CS crystals grown using newly purified protein sample that resolved the tetrameric assembly from a higher molecular weight CS species. A. Hexagonal plate morphology obtained in NaCl/citrate crystallization conditions. B. Hexagonal prism morphology obtained in NaCl/citrate/gycerol crystallization conditions. C. Cluster of needles and thin plates from malonate crystallization conditions.

Continue crystallization optimization employing the new CS tetramer-only samples yielded visually better crystals (i.e., better defined crystal faces and edges, fewer visual defects). Additionally, maximum crystal sizes significantly increased (~0.45 mm vs. ~0.30 mm maximum dimension). Both of these properties suggest increased microscopic order within these new crystals (Figure 16). Additionally, we have recently identified crystallization conditions similar to these NaCl-based condition except with the inclusion of 10-15% glycerol. This may improve the crystals by several different mechanisms. First, glycerol is a cryoprotectant, so inclusion in the crystallization cocktail reduces or eliminates potentially osmotically shocking crystals through addition post-crystal growth. Additionally, glycerol can stabilize protein folding, especially alpha-helical regions, and enhance solubility. Thus, its inclusion in the crystallization cocktail may aid crystal quality.

We have demonstrated significant progress in CS crystallization optimization for the purpose of obtaining a high-resolution X-ray crystal structure useful for antibacterial drug design efforts. Based upon this progress, we expect to obtain this structure soon. If additional optimization is required, several additional strategies exist. Surface entropy reduction (SER) is based on the observation that entropic *hot spots* on a protein's surface (e.g., clusters of long flexible polar side chains) tend to inhibit crystallization. Analysis of *A. baumannii* CS predicts three such high-entropy surface patches (residues 56-66, 90-93 and 165-167), and suggests several residues within each patch for mutation to residues (e.g., Ala) that should lower the local entropy and thus be more amenable to forming high-quality crystals. We are also exploring the engineering of *crystallization epitopes* into CS. The concept of crystallization epitopes has recently been developed by John Hunt (Columbia Univ.; personal communication), and involves mutation of surface-exposed residues present in alpha-helical structures in order to reduce surface entropy

while retaining overall protein solubility and stability by forming n, n+4 salt bridges. Additionally, the expected availability of the 5-enolpyruvylshikimate-3-phosphate (EPSP, unavailable commercially), isolated from the coupled reaction using SK and PD-PSCVT, may provide a useful tool for crystallization trials, as often binding of a substrate results in stabilization of protein conformation. A related strategy is the use of *additive* screens (e.g., Hampton Research Silver Bullets Additives) to improve crystal quality. The guiding rational for conducting additive screens is that crystallization is driven by the previously identified conditions, with the addition of minor amounts of other components (e.g., a variety of ions, common biologically relevant small molecules/cofactors, di- and tri-peptides, etc.) then allows for the identification of components that directly or indirectly stabilize regions of the target protein to improve crystal quality.

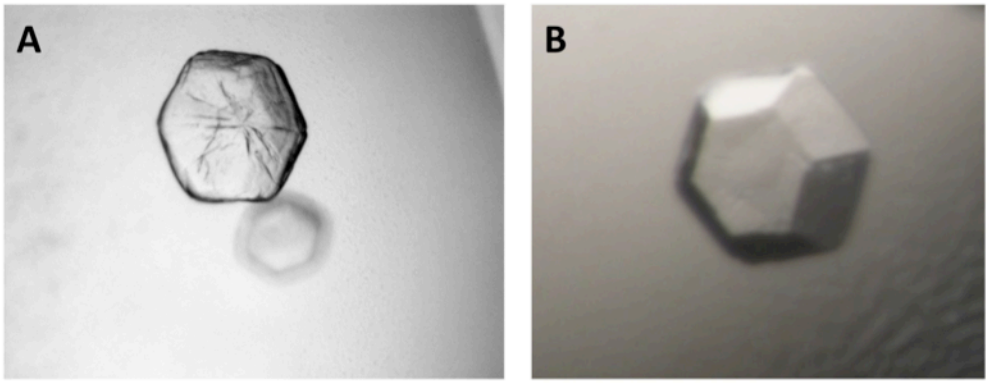


**Figure 16**. CS crystals. A. Example of a crystal grown using CS obtained using the original purification protocol, which does not resolve tetrameric CS from higher oligomeric and possibly misfolded or aggregated CS. B. Crystals grown using CS obtained from the new purification protocol, which yields primarily tetrameric CS.

### Goal 2. Characterization of a Novel NRPS Biosynthetic Cluster

The non-ribosomal peptide synthetases (NRPSs) are a family of large, modular enzymes that produce peptides with important activities (*8, 9*). NRPS products are diverse, incorporating as many as 100 different substrate amino acids and exhibiting additional chemical modifications including glycosylations, cyclizations, and halogenations. The products play important roles in microbial pathogenesis, including nutrient acquisition, intercellular communication, and exhibiting antibiotic activity. While novel NRPS natural products have been identified in soil and marine bacterial species, there has been limited effort to characterize the small NRPS clusters that are present in many human pathogens.

We identified an operon in *A. baumannii* that we wished to target to expand our investigation into NRPS synthesis of novel natural products. The operon encompasses eight genes that are co-transcribed (Table 3, blue). Upstream of the synthetic operon is an acyl-HSL synthase, an enzyme involved in synthesis of quorum signaling homoserine lactones. Immediately upstream of these genes encoding the synthetic operon is a homolog of the *P. aeruginosa* PhzR/LasR transcriptional regulators that are involved in quorum-sensor regulation (*10*). It is therefore highly likely that the ABBFA_003407 protein is involved in the quorum signal-dependent regulation of this operon (*11*).

Table 3. The targeted ABBFA_003406 NRPS operon of *A. baumannii*.

| | Function | AB307-0294 | Status |
|---|---|---|---|
| 1 | Acyl-HSL Synthase (*abaI* or *cepI*) | ABBFA_003409 | |
| 2 | Hypothetical | ABBFA_003408 | |
| 3 | PhzR-type Regulator | ABBFA_003407 | |
| 4 | NRPS (Self-standing Adenylation Domain) | ABBFA_003406 | Cloned, Purified, Biochemically analyzed |
| 5 | Acyl-CoA dehydrogenase | ABBFA_003405 | Cloned, expressed |
| 6 | NRPS (Self-standing Peptidyl Carrier Protein) | ABBFA_003404 | Cloned, Purified, Biochemically Analyzed, Crystallized, Structure Determined |
| 7 | NRPS (Condensation-Adenylation-PCP-Thioesterase) | ABBFA_003403 | Cloned, Purified, Biochemically Analyzed, Small Crystals |
| 8 | RND Transporter | ABBFA_003402 | Cloned |
| 9 | Hypothetical | ABBFA_003401 | Cloned |
| 10 | Bifunctional Dehydratase / esterase | ABBFA_003400 | Cloned, Expressed |
| 11 | Phosphopantetheinyl transferase (PPTase) | ABBFA_003399 | Not targeted at this time |

Genes are numbered consecutively. The proteins of the operon of interest are listed in blue. The upstream genes that are likely to be involved in regulation are included in black. The presumed function is listed based on sequence homology. Gene and Protein names from two strains are reported. In the ATCC17978 strain, the gene names are A1S_0109 through A1S_0119.

Within this NRPS operon are eight proteins. One, ABBFA_003402, is a RND transporter that is likely involved in efflux of the natural product. Another, ABBFA_003399, is a phosphopantetheinyl transferase (*12*), an enzyme that post-translationally modifies the acyl carrier protein domains of two of the NRPS proteins to convert from their inactive *apo* to the active *holo* state. The remaining six proteins therefore form the synthetic operon.

We have focused our attention this year on two aspects, the development of a bioassay that will enable us to isolate and characterize the signaling molecule produced by the NRPS cluster and the structural and functional characterization of the enzymes from this pathway.

**Development of a Quantitative Bioassay**

A significant advance early this year came not from our lab but instead from a report in the literature that tied the genes encoding this NRPS pathway to a phenotype. The report by Rather and colleagues (*11*) identified motility in *A. baumannii* strains when grown on low percentage agar. The exact morphology of the colony was dependent on both the *A. baumannii* strain as well as the source of the agar, with observations of outward growth of concentric rings, often containing small projections or “a manner that resembled branching tentacles”. A directed assessment of the involvement of the *pilT* and *abaI* genes demonstrated the involvement of pilus formation and quorum signaling as playing a role in this *A. baumannii* motility. The authors then screened random mutants for other genes that played a role in motility and identified seven genes that, upon disruption, resulted in decreases in motility to values that were 20-70% of the wild-type (as measured by the radius of colony growth). Among the seven genes were the homologs of ABBFA_003405 and ABBFA_003403, two genes of the NRPS operon that we are studying. The authors also noted that this operon was transcriptionally activated by the *A. baumannii* quorum signal, 3-hydroxy-dodecanoyl-homoserine lactone (3OH-$C_{12}$-HSL). A more recent report was published this summer that also demonstrates a potential role of this NRPS pathway in *A. baumannii* biofilms (*13*). In this study, it was shown through whole transcriptome analysis that this NRPS operon is among the most highly differentially regulated, with very low– and in one case, no–expression in planktonic or stationary phase cells compared with cells from a biofilm. Additionally, a mutation in the ABBFA_003404 gene, encoding the peptidyl carrier protein that we have structurally characterized, resulted in compromised biofilm formation in a quantitative assay.

These exciting results tied the natural product from the ABBFA_003406 NRPS cluster to motility and biofilm formation, two phenotypes that are associated with virulence in gram negative bacteria (*14, 15*). Additionally, it allows us to develop a bioassay that we hope to use to isolate the active molecule that is produced by the ABBFA_003406 NRPS cluster. We obtained the M2 (wild-type), M2-2, and M2-11 strains from Dr. Rather and have used them to develop this assay. The M2-2 and M2-11 strains harbor disruptions in ABBFA_003405 and ABBFA_003403, respectively. (Note that the homologs of these genes in the ATCC 17978 strain used by both Clemmer (*11*) and Rumbo-Feal (*13*) are A1S_0113 and A1S_0115, respectively). We have developed a bioassay that will be amenable to our efforts to isolate the active component.

Following the protocol described by Clemmer, low percentage (0.3%) agar plates are used to monitor *A. baumannii* growth. Cells from an overnight culture (1 µl) are added to the center of the plate, and the colony growth is monitored. To develop a quantitative assay, we tested multiple variables, including media, agar source, agar concentration, and phase of growth of the inoculum (log phase and saturated cultures). We found that choice of agar was critical with the Eiken agar (Eiken Chemical Co., Japan) showing most consistent results. After several experiments to qualitatively monitor growth, we created a ruler of concentric rings that allowed us to measure both the "internal" radius of the colony growth, as well as the external radius that measured the farthest projection (Figure 17). These values were plotted and illustrated that the mutant cell lines consistently grew at a rate of ~80-90% of the wild-type cells. We are continuing our efforts to optimize this assay and hope to find conditions that further enhance the difference in magnitude between the wild-type and mutant cells.

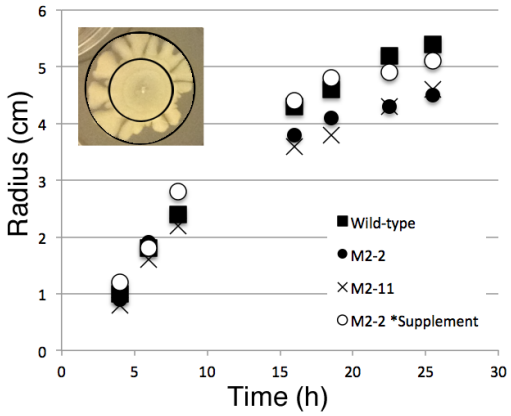


**Figure 17**. Analysis of colony growth for wild-type and mutant strains of *A. baumannii*. Using the Eiken agar, the colony grew as a larger central core that showed projections. We measured both the inner and outer radii of growth (represented by the two rings in the inset) over the course of 24h. The graph shows the plot of the outer radius for wild-type (squares), the two mutants (circles and crosses) and a mutant strain supplemented with media from the wild-type cell line (open circles).

Importantly, we also isolated media from the wild-type culture, removed the cells by centrifugation, and repeated the growth experiment with 1 µl of the M2-2 mutant as well as 1 µl of the conditioned media (open circles). This colony grew at the same rate as the wild-type cell line, suggesting that the wild-type culture is able to produce the signaling molecule that can induce the higher motility.

The assay is now set to search for a fraction of the conditioned media from wild-type cells that is able to induce the higher motility. During this past year, while we were optimizing this bioassay, we did preliminary experiments with the HPLC to fractionate the media. During these experiments, we were hoping that we might be able to observe a significant difference in the metabolite profiles of the wild-type and mutant strains. The absence of a peak in the mutant cell

lines might give us clues as to the identity of the NRPS product. We grew the *A. baumannii* strains in succinate minimal media. Extractions in ethyl acetate, chloroform, and hexane were attempted and yielded no detectable signal; all compounds remained in the aqueous layer. Small differences have been observed in cultures of different volumes, suggesting that cell density or growth profile may impact metabolite production (not shown).

Multiple experimental runs have been performed with the wild-type and mutant strains, supplemented with acyl-homoserine lactone to induce this operon (*11*) or glycine. Glycine, the substrate for ABBFA_003403, was included as increased availability may drive the secondary metabolite pathway toward product formation, as has been observed with alternate natural product pathways. Small differences have been observed in multiple runs and are being explored further (Figure 18).

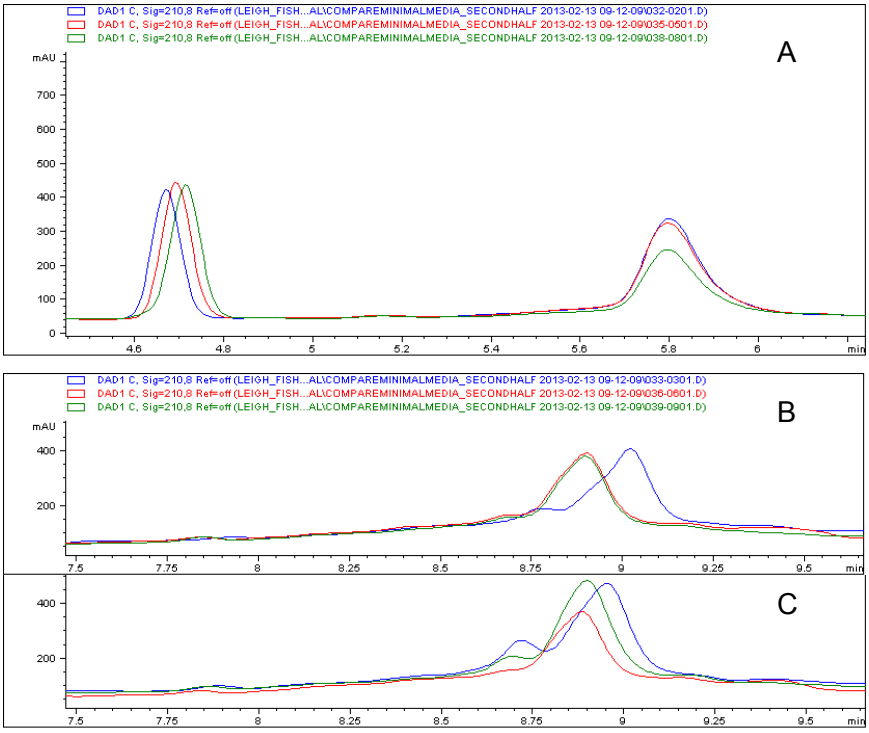


**Figure 18**. HPLC chromatograms of *A. baumannii* metabolites. Portions of a metabolite profile from M2 (blue), M2-2 (red), and M2-11 (green). A. Growth in SM9 media. B. Growth supplemented with HSL. C. Growth supplemented with glycine.

We are now in position to combine the two experiments, the bioassay and the metabolite fractionation, to initiate our attempts to isolate the active NRPS product. We will first grow wild-type cells in minimal media to see if we can repeat the supplementation assay of Figure 17. The ability to perform this in minimal media will reduce the complexity of the starting material from which we are isolating the active compound.

**Biochemical and Structural Characterization of Proteins from the NRPS Cluster**

Last year, we reported on the structure determination of ABBFA_003404, the carrier protein that likely serves as the substrate for the ABBFA_003406 adenylation domain. We have optimized purification of ABBFA_003406 and demonstrated the relative lability of the protein. This observation allowed us to improve the substrate specificity assay and identify that threonine serves as an optimal substrate in the pyrophosphate exchange assay. The prior preparations were showing high levels of background catalytic activity, suggesting that the adenylation domain was co-purifying with a potential carboxylate substrate. We have seen this previously

both with fatty acyl-CoA synthetase, a related adenylate-forming enzyme within the ANL superfamily of enzymes (Reger, Thesis Dissertation, 2008, University at Buffalo) and with the PvdQ fatty acyl hydrolase from *P. aeruginosa* (*16*). Our efforts to remove the co-purifying substrate by extensive dialysis were unsuccessful, given the marginal stability of the protein. Similarly, efforts to remove the contaminant by driving the alternate substrate off by catalytic reaction with the co-substrates ATP and a non-specific acceptor such as hydroxylamine also proved unsuccessful.

We therefore returned to the purification to attempt to isolate quickly and efficiently the a3406 adenylation domain for assays. An improved protocol that rapidly progressed through both chromatographic steps was developed. A gel filtration step again demonstrates multiple peaks, suggesting that we are still fighting aggregation. However, the peak that runs as a dimer appears better behaved and was used for substrate specificity studies with the pyrophosphate exchange assay. Higher activity was obtained, and the activity now seems to be optimal with the small hydroxyl containing amino acids threonine and serine.

These substrates were additionally used in the biochemical assay. This assay would use the PCP domain, ABBFA_003404 as a substrate for the reaction and detects the steady-state production of AMP. Unfortunately, to date we have been unable to detect activity in this assay. We are continuing to explore the function in this and other assays.

## Key Research Accomplishments

Building on our progress from the first year of our award, we have accomplished the following tasks that contribute towards goals of the project during the period of November 2012 through October 2013.

Goal 1. Preliminary data have established that chorismate synthase and prephenate dehydrogenase/3-phosphoshikimate-1-carboxyvinyl transferase are essential proteins for *A. baumannii* infection. Therefore our hypothesis is that these proteins are potential therapeutic targets. The object of this goal is to validate these proteins in the chorismate biosynthesis pathway as therapeutic targets.

- The structure of Shikimate Kinase was solved to 2.1 Å that shows shikimate present in the active site of the enzyme (Monthly Report #17). Final refinement is presented in Report #20.
- Enzymatic synthesis of shikimate-3-phosphate and isolation by chromatographic separation (Report #18). The identity of the compound was confirmed with mass spectrometry, showing that there is contamination with ATP and ADP (Report #19).
- We have generated site-specific disruption of the *aroC* gene in three strains of *A. baumannii*, AB307-0297, AB714, and AB764 (Report #20).
- The three strains are unable to grow in human ascites, demonstrating *ex vivo* essentiality (Report #20).
- Improved purification protocol of CS was developed, allowing growth of improved crystals (Report #20)
- The three *aroC* mutant strains show growth in rat abscess model; however the wild-type growth was lower than expected (Report #21).
- Biochemical activity of the PSCVT domain of PD-PSCVT bifunctional protein was demonstrated by detecting phosphate formation, using a coupled assay with shikimate kinase (Report #21).
- The isolated PSCVT domain was crystallized (Report #21)
- The *aroA* gene has been sequenced from strains AB932 (Report #22) and AB1013 (Report #23) showing two and zero mutations that influence protein coding, respectively.
- The *aroA* gene with surrounding flanking sequences has been cloned and used to generate an *aroA*::*kan* cassette that will be used for creating disruptions of *aroA* in *A. baumannii* (Report #23)
- The structure of the PSCVT domain has been solved (Report #23).
- The *aroA*::*kan* cassette was cloned into the suicide vector pKNG101 (Report #24).
- Differential scanning fluorimetry demonstrates the binding of substrate shikimate to shikimate kinase (Report #24).

Goal 2. Characterize a novel natural product synthetic pathway encoded by an *A. baumannii* Non-Ribosomal Peptide Synthetases pathway. Our hypothesis is that this cluster is responsible for the production of a novel compound that may impact growth or virulence of *A. baumannii*.

- Strains of *A. baumannii* harboring disruptions in the targeted NRPS operon were obtained from the lab of Dr. Philip Rather, allowing us to continue our studies without the need to generate directed disruption mutants as we had originally proposed (Report #13).

- The growth phenotype of the M2 strain of *A. baumannii* was reproduced, demonstrating slower colony migration of the M2-11 strain (Report #15)
- ABBFA_003400, ABBFA_003401, and ABBFA_003405 were expressed solubly (Report #17). ABBFA_003400 has been purified to homogeneity and is in crystallization trials (Report #19)
- A protocol to fractionate culture supernatants via HPLC was developed that identified small, reproducible changes in metabolite profiles (Report #18).
- Protein ABBFA_003406 purification was optimized for activity (Report #20), showing an improved amino acid substrate specificity profile (Report #22).
- Protein ABBFA_003403, the four domain NRPS protein was crystallized in the presence of the glycyl-adenosyl vinylsulfonamide inhibitor (Report #22).
- Developed a quantitative bioassay for *A. baumannii* motility in low percentage Eiken agar plates. Demonstrated that addition of culture supernatant from wild-type cells confers higher motility on the M2-11 mutant strain, harboring a disruption in the equivalent of ABBFA_003403 (Report #23).

## Reportable Outcomes

The following publication was supported by this award.

Russo, T. A., Beanan, J. M., Olson, R., MacDonald, U., Cox, A. D., St. Michael, F., Vinogradov, E. V., Spellberg, B., Luke-Marshall, N. R., and Campagnari, A. A. (2013) Te K1 Capsular Polysaccharide from *Acinetobacter baumannii* is a Potential Therapeutic Target via Passive Immunization. *Infection and Immunity* 81, 915-922.

This publication is attached in the appendices.

Dr. Russo also co-authored a book chapter relevant to this project.

**Russo, T.A.** and Johnson J.R. Diseases caused by gram-negative enteric bacilli. In: Harrison's Principles of Internal Med., 19th Ed. Chapter 184. *In Press.*

Posters

Timothy C. Umland, Joseph R. Luft, Eleanor Cook, George T. DeTitta, Angela M. Lauricella, Raymond M. Nagel, Edward H. Snell, Jennifer R. Wolfley, "High-throughput crystallization of cytosolic and membrane proteins to structurally enable drug discovery," The 7th Drug Design and Medicinal Chemistry Conference. Boston, MA, May 8-10, 2013.

L. Wayne Schultz, Joseph R. Luft, Eleanor Cook, George T. DeTitta, Angela M. Lauricella, Raymond M. Nagel, Edward H. Snell, Jennifer R. Wolfley, "High-throughput crystallization of cytosolic and membrane bound proteins" Cambridge Healthtech Institute 8th Annual Drug Discovery Chemistry Conference. San Diego, CA, April 16-18, 2013. Abstract #212.

L. Wayne Schultz, Thomas Russo, Jennifer Breen, Jessica Kocsis, Timothy C. Umland "Structural Biology of the Shikimate Pathway in Multi-drug Resistant Gram Negative Bacteria", Annual Meeting of the American Crystallographic Association. Honolulu, HI, July 22, 2013. Abstract #1578.

Nathan Roach, Jesica Kocsis, and Timothy Umland, "The Purification and Crystallization of *Acinetobacter baumannii* Chorismate Synthase," University at Buffalo Biomedical Research Day. Buffalo, NY August 2, 2013.

Kristin Sutton, Thomas Russo, Jennifer Breen, Jessica Kocsis, Timothy C. Umland, L. Wayne Schultz "Structural Biology of the Shikimate Pathway in Multi-drug Resistant Gram Negative Bacteria" The 74th Annual Pittsburgh Diffraction Conference. Buffalo, NY, September 19, 2013. Abstract #P21.

C.L. Allen and A.M. Gulick. "Investigation of non-ribosomal peptide synthetase-related genes from an uncharacterized operon implicated in *Acinetobacter baumannii* motility" 23rd Enzyme Mechanisms Conference, Coronado CA. January 2013.

The following protein structure dataset, including atomic coordinates and structure factors, was deposited with the Protein Data Base (http://www.pdb.org) using funds from this award.

**4HKQ**, *Crystal Structure of Free-Standing Peptidyl Carrier Protein from Uncharacterized Acinetobacter baumannii Secondary Metabolic Pathway*. Released Oct 2013.

## Conclusions

*A. baumannii* remains a significant biomedical problem that is increasingly being recognized as a cause of nosocomial infections in a wide variety of health care settings (*17*). The prevalence of resistant strains of *A. baumannii (18, 19)* and the current lack of effective treatments suggests a pressing need for novel approaches to identify and validate new targets for antibiotic treatments. We continue to pursue two complementary approaches to address this problem that comprise the aims of this research project and together will identify, characterize, and validate novel antibiotic targets in *A. baumannii*.

We have implemented the strategy of investigating *in vivo* essential genes (i.e., essential for growth and survival during infection of a host) to advance the traditional antibacterial drug development pipeline in order to achieve the first goal of this project. Our methodology for screening and validating *in vivo* essential genes identified *A. baumannii* targets that previously were largely overlooked as antibacterial targets (*2*), including CS and PD-PSCVT. In the second goal, we are making an investment in the understanding of the fundamental microbial physiology of this pathogen. Towards this end, we have initiated the investigation of a novel natural product biosynthetic pathway that has been implicated in bacterial motility. These genes encoding this pathway are upregulated in response to a bacterial quorum signal. We aim to identify this novel compound and understand its role in infection and virulence.

During the current project period, we made significant advances in the area of *A. baumannii* genetics. We observed that in many strains of *A. baumannii*, creating directed gene knockouts was difficult, thus impeding our goal of confirming the *in vivo* essentiality of the CS and PD-PSCVT targets. We have developed and optimized protocols for improving directed gene knockout efficiency that will be useful for this project but also to the general *A. baumannii* community. We are currently establishing the *in vivo* essentiality of our targets across multiple *A. baumannii* strains.

We have determined the crystal structure of PD-PSCVT at a resolution sufficient for use in fragment-based lead discovery methods. Additionally, we have determined the crystal structure of SK, the enzyme preceding the PSCVT in the shikimate pathway, and which may also serve as antibacterial target. Obtaining diffraction quality CS has been more difficult than initially estimated. We have made sufficient progress in improving the crystal quality and are confident we will obtain a CS structure soon. We are progressing into fragment-based methods for identifying small molecules that may serve as antibacterial leads against these targets. We will place particular emphasis on any fragments that exhibit binding to multiple targets, as these compounds have the potential to be developed into multi-target inhibitors, thereby reducing the likelihood of the development of resistant mutants.

To accompany and validate the structural studies, we have developed activity assays for PD-PSCVT and SK that are now being used to identify and evaluate small molecules as potential antibacterial leads. The substrate for CS is not commercially available. We are developing a SK→PD-PSCVT→CS coupled reaction to monitor CS activity as an end-point assay.

We have made important progress in understanding the natural product produced by the identified non-ribosomal peptide synthetase cluster, having cloned and produced the synthetic enzymes and identified the molecular building blocks. The acquisition this year of the mutant strains harboring disruptions in the NRPS biosynthetic operon has allowed us to examine the phenotype of bacterial motility and to develop a bioassay that we can use to isolate the active molecule. We have additionally improved on the production and purification of the synthetic enzymes and have recently improved on our substrate specificity assay, which we believe is providing new insights into the potential product.

## References


1. Russo, T. A., MacDonald, U., Beanan, J. M., Olson, R., MacDonald, I. J., Sauberan, S. L., Luke, N. R., Schultz, L. W., and Umland, T. C. (2009) Penicillin-binding protein 7/8 contributes to the survival of Acinetobacter baumannii in vitro and in vivo, *J Infect Dis 199*, 513-521.
2. Umland, T. C., Schultz, L. W., Macdonald, U., Beanan, J. M., Olson, R., and Russo, T. A. (2012) In Vivo-Validated Essential Genes Identified in Acinetobacter baumannii by Using Human Ascites Overlap Poorly with Essential Genes Detected on Laboratory Media, *mBio 3*.
3. Roberts, C. W., Roberts, F., Lyons, R. E., Kirisits, M. J., Mui, E. J., Finnerty, J., Johnson, J. J., Ferguson, D. J., Coggins, J. R., Krell, T., Coombs, G. H., Milhous, W. K., Kyle, D. E., Tzipori, S., Barnwell, J., Dame, J. B., Carlton, J., and McLeod, R. (2002) The shikimate pathway and its branches in apicomplexan parasites, *J Infect Dis 185 Suppl 1*, S25-36.
4. Blanco, B., Prado, V., Lence, E., Otero, J. M., Garcia-Doval, C., van Raaij, M. J., Llamas-Saiz, A. L., Lamb, H., Hawkins, A. R., and Gonzalez-Bello, C. (2013) Mycobacterium tuberculosis shikimate kinase inhibitors: design and simulation studies of the catalytic turnover, *J Am Chem Soc 135*, 12366-12376.
5. Gu, Y., Reshetnikova, L., Li, Y., Wu, Y., Yan, H., Singh, S., and Ji, X. (2002) Crystal structure of shikimate kinase from Mycobacterium tuberculosis reveals the dynamic role of the LID domain in catalysis, *J Mol Biol 319*, 779-789.
6. Funke, T., Healy-Fried, M. L., Han, H., Alberg, D. G., Bartlett, P. A., and Schonbrunn, E. (2007) Differential inhibition of class I and class II 5-enolpyruvylshikimate-3-phosphate synthases by tetrahedral reaction intermediate analogues, *Biochemistry 46*, 13344-13351.
7. Matulis, D., Kranz, J. K., Salemme, F. R., and Todd, M. J. (2005) Thermodynamic stability of carbonic anhydrase: measurements of binding affinity and stoichiometry using ThermoFluor, *Biochemistry 44*, 5258-5266.
8. Giessen, T. W., and Marahiel, M. A. (2012) Ribosome-independent biosynthesis of biologically active peptides: Application of synthetic biology to generate structural diversity, *FEBS Lett 586*, 2065-2075.
9. Strieker, M., Tanovic, A., and Marahiel, M. A. (2010) Nonribosomal peptide synthetases: structures and dynamics, *Curr Opin Struct Biol 20*, 234-240.
10. Khan, S. R., Herman, J., Krank, J., Serkova, N. J., Churchill, M. E., Suga, H., and Farrand, S. K. (2007) N-(3-hydroxyhexanoyl)-l-homoserine lactone is the biologically relevant quormone that regulates the phz operon of Pseudomonas chlororaphis strain 30-84, *Appl Environ Microbiol 73*, 7443-7455.
11. Clemmer, K. M., Bonomo, R. A., and Rather, P. N. (2011) Genetic analysis of surface motility in Acinetobacter baumannii, *Microbiology 157*, 2534-2544.
12. Lambalot, R. H., Gehring, A. M., Flugel, R. S., Zuber, P., LaCelle, M., Marahiel, M. A., Reid, R., Khosla, C., and Walsh, C. T. (1996) A new enzyme superfamily - the phosphopantetheinyl transferases, *Chem Biol 3*, 923-936.
13. Rumbo-Feal, S., Gomez, M. J., Gayoso, C., Alvarez-Fraga, L., Cabral, M. P., Aransay, A. M., Rodriguez-Ezpeleta, N., Fullaondo, A., Valle, J., Tomas, M., Bou, G., and Poza, M. (2013) Whole Transcriptome Analysis of Acinetobacter baumannii Assessed by RNA-Sequencing Reveals Different mRNA Expression Profiles in Biofilm Compared to Planktonic Cells, *PLoS One 8*, e72968.
14. Burrows, L. L. (2012) Pseudomonas aeruginosa Twitching Motility: Type IV Pili in Action, *Annu Rev Microbiol 66*, 493-520.

15. McConnell, M. J., Actis, L., and Pachon, J. (2013) Acinetobacter baumannii: human infections, factors contributing to pathogenesis and animal models, *FEMS Microbiol Rev 37*, 130-155.
16. Drake, E. J., and Gulick, A. M. (2011) Structural characterization and high-throughput screening of inhibitors of PvdQ, an NTN hydrolase involved in pyoverdine synthesis, *ACS Chem Biol 6*, 1277-1286.
17. Visca, P., Seifert, H., and Towner, K. J. (2011) Acinetobacter infection--an emerging threat to human health, *IUBMB life 63*, 1048-1054.
18. Cerqueira, G. M., and Peleg, A. Y. (2011) Insights into Acinetobacter baumannii pathogenicity, *IUBMB life 63*, 1055-1060.
19. Peleg, A. Y., Seifert, H., and Paterson, D. L. (2008) Acinetobacter baumannii: emergence of a successful pathogen, *Clin Microbiol Rev 21*, 538-582.

## Appendices

We have attached the following publication that resulted from research supported by this award.

Russo, T. A., Beanan, J. M., Olson, R., MacDonald, U., Cox, A. D., St. Michael, F., Vinogradov, E. V., Spellberg, B., Luke-Marshall, N. R., and Campagnari, A. A. (2013) Te K1 Capsular Polysaccharide from *Acinetobacter baumannii* is a Potential Therapeutic Target via Passive Immunization. *Infection and Immunity* 81, 915-922.

IAI Journals.ASM.org

# The K1 Capsular Polysaccharide from *Acinetobacter baumannii* Is a Potential Therapeutic Target via Passive Immunization

**Thomas A. Russo,[a,d] Janet M. Beanan,[b,d] Ruth Olson,[b,d] Ulrike MacDonald,[b,d] Andrew D. Cox,[e] Frank St. Michael,[e] Evgeny V. Vinogradov,[e] Brad Spellberg,[f] Nicole R. Luke-Marshall,[c,d] Anthony A. Campagnari[c,d]**

Veterans Administration Western New York Healthcare System,[a] Department of Medicine,[b] Department of Microbiology and Immunology,[c] and The Witebsky Center for Microbial Pathogenesis,[d] University at Buffalo-State University of New York, Buffalo, New York, USA; Institute for Biological Sciences, National Research Council of Canada, Ottawa, Ontario, Canada[e]; Division of General Internal Medicine, Los Angeles Biomedical Research Institute at Harbor-University of California Los Angeles Medical Center, Torrance, California, USA[f]

**The emergence of extremely resistant and panresistant Gram-negative bacilli, such as *Acinetobacter baumannii*, requires consideration of nonantimicrobial therapeutic approaches. The goal of this report was to evaluate the K1 capsular polysaccharide from *A. baumannii* as a passive immunization target. Its structure was determined by a combination of mass spectrometric and nuclear magnetic resonance (NMR) techniques. Molecular mimics that might raise the concern for autoimmune disease were not identified. Immunization of CD1 mice demonstrated that the K1 capsule is immunogenic. The monoclonal antibody (MAb) 13D6, which is directed against the K1 capsule from *A. baumannii*, was used to determine the seroprevalence of the K1 capsule in a collection of 100 *A. baumannii* strains. Thirteen percent of the *A. baumannii* isolates from this collection were seroreactive to MAb 13D6. Opsonization of K1-positive strains, but not K1-negative strains, with MAb 13D6 significantly increased neutrophil-mediated bactericidal activity *in vitro* ($P < 0.05$). Lastly, treatment with MAb 13D6 3 and 24 h after bacterial challenge in a rat soft tissue infection model resulted in a significant decrease in the growth/survival of a K1-positive strain compared to that of a K1-negative strain or to treatment with a vehicle control ($P < 0.0001$). These data support the proof of principle that the K1 capsule is a potential therapeutic target via passive immunization. Other serotypes require assessment, and pragmatic challenges exist, such as the need to serotype infecting strains and utilize serotype-specific therapy. Nonetheless, this approach may become an important therapeutic option with increasing antimicrobial resistance and a diminishing number of active antimicrobials.**

*Acinetobacter baumannii* has become a pathogen of increasing medical importance (1, 2). The majority of *A. baumannii* infections have been acquired in health care facilities (3–5). The respiratory tract, particularly in ventilated patients, the urinary tract, the bloodstream, intravascular devices, surgical sites (including sites of postneurosurgical meningitis), and decubitus or diabetic ulcers are favored sites of infection (6, 7). *A. baumannii* has also been shown to cause infections outside the health care setting, namely, severe community-acquired pneumonia (usually in alcoholics) (8–10) and infections in war-related injuries and in tsunami survivors (11, 12). Mortality rates associated with *A. baumannii* infection range from 19 to 54% (13).

Particularly worrisome is the significant degree of antimicrobial resistance demonstrated by many strains of *A. baumannii* (14, 15). The prevalence of multiresistance (resistance to three or more classes of antimicrobials), extreme resistance (resistance to all but one or two classes of antimicrobials), and panresistance (resistance to all antimicrobials) is increasing (16, 17).

Thus, treatment of infections due to *A. baumannii* has become challenging. Unfortunately, as of 2009 there were virtually no new antimicrobial agents active against Gram-negative bacilli (GNB) in the pharmaceutical pipeline (18). A 2011 update found some antimicrobials that had activity against GNB in development, but none have reached phase 3 trials (19, 20). Some combination of the development of new antimicrobial agents and nonantimicrobial approaches to treatment is needed. One approach worthy of consideration is the use of passive immunization. Historically this approach has been used primarily for toxin-mediated disease (e.g., snake or tetanus toxins) and viral infections (e.g., rabies or varicella-zoster virus) (21, 22). Although passive immunization (treatment with specific or nonspecific immunoglobulin preparations) provides only temporary immunity, it may be sufficient to clear an acute infection alone or in combination with antimicrobials that possess less than optimal efficacy. Recently, anti-OmpA antibodies were shown to confer protection against extremely antimicrobial-resistant *A. baumannii* in a mouse bloodstream infection model (23), justifying the potential of this approach for *A. baumannii*.

Capsular polysaccharides often possess the desirable characteristics of an antigenic target such as surface exposure, broad prevalence among clinical isolates, generation of a protective immune response, and a role in the pathogenesis of disease. Further, capsules have formed the basis for several successful vaccines directed against extracellular bacterial pathogens such as *Haemophilus influenzae* type b, *Streptococcus pneumoniae*, and certain serotypes of *Neisseria meningitidis* (24–27). Although not as efficacious, a vac-

**Received** 2 November 2012 **Returned for modification** 2 December 2012
**Accepted** 24 December 2012
**Published ahead of print** 7 January 2013
**Editor:** J. B. Bliska
Address correspondence to Thomas A. Russo, trusso@acsu.buffalo.edu.
Supplemental material for this article may be found at http://dx.doi.org/10.1128/IAI.01184-12.

doi:10.1128/IAI.01184-12

cine based on the Vi capsular polysaccharide is approved for *Salmonella typhi* (28). A potential limitation of active immunization with nonzwitterionic polysaccharides is the development of a T-independent response that is characterized by a poor memory response, particularly in the very young and old (29). However, the development of conjugated vaccines has for the most part overcome this drawback (30). Therefore, we hypothesized that capsular polysaccharides of *A. baumannii* would make an ideal antigenic target for protection against or treatment of infection, using either an active or passive immunization approach. Remarkably little is known about the prevalence and antigenic variation of capsular polysaccharides in *A. baumannii*. Presumably most clinical isolates possess a capsule since its loss severely decreases virulence (31); however, this has not been systematically established. Further, the number and prevalence of capsular serotypes in clinical *A. baumannii* isolates are also unknown. Studies assessing seroprevalence and evaluating specific capsular serotypes for their potential as active or passive immunization targets are needed.

Our laboratory is in the process of filling these knowledge gaps. To date, we have established that the K1 capsular polysaccharide from the *A. baumannii* strain AB307-0294 is surface exposed and is a virulence factor (31). However, no data are available on its seroprevalence, its immunogenicity, and the ability of antibodies directed against the capsular polysaccharide from *A. baumannii* to confer protection against infection. In this report those critical criteria for a vaccine candidate were assessed. Further, the structure of the K1 capsule was also delineated to determine whether any epitopes resembled human antigens. The results obtained support the hypothesis that *A. baumannii* capsular polysaccharides warrant continued evaluation as potential targets for active and/or passive immunization.

## MATERIALS AND METHODS

**Bacterial strains and media.** *A. baumannii* strain AB307-0294 (blood isolate, sequence type 15 [ST15], clonal group 1 based on work by Ecker et al. [32]) is an encapsulated isolate from a patient hospitalized at Erie County Medical Center, Buffalo, NY, in 1994 (33). Capsule serotypes have not been defined in *A. baumannii*. Therefore, we have designated the capsular serotype present in AB307-0294 as K1. AB307.30 is an isogenic K1-negative derivative of AB307-0294 that possesses a disruption in *ptk*, which encodes a putative protein tyrosine kinase (PTK) (31). *A. baumannii* strains 693, 715, and 803 are K1 capsule positive, were obtained from the Walter Reed Army Medical Center (WRAMC, kindly provided by David Craft and Paul Scott), and were used in opsonophagocytosis studies. *A. baumannii* strain AB979 is K1 capsule negative, was also obtained from the WRAMC, and was used in the rat soft tissue infection model studies (34). The collection of 100 strains used for seroprevalence studies are listed in Table S1 in the supplemental material with their STs and sites of isolation when delineated. These *A. baumannii* strains were obtained from the WRAMC (78), Buffalo, NY (11), Los Angeles, CA (5), Chicago, IL (2), Cleveland, OH (1), and the ATCC (3). Strains were grown in Luria-Bertani (LB) medium unless stated otherwise and maintained at −80°C in 50% LB broth and 50% glycerol.

**Determination of the K1 capsule structure.** Polysaccharides were isolated from AB307-0294 (wild type, K1 capsule positive) and AB307.30 (isogenic derivative of AB307-0294, capsule negative) by standard phenol-water extraction (35). Structural elucidations were performed on the purified high-molecular-weight capsular polymer, isolated following anion-exchange chromatography as described previously (36). Capillary electrophoresis electrospray mass spectrometry (CE-ES-MS) and nuclear magnetic resonance (NMR) spectroscopy experiments were performed as described previously (37).

**Generation and production of the MAb 13D6, which is specific for the K1 capsule expressed in AB307-0294.** Monoclonal antibodies (MAbs) were developed and screened as described previously (38, 39). In brief, two BALB/c mice were injected intraperitoneally with a sublethal dose ($1 \times 10^4$ CFU) of live AB307-0294 (K1 positive) without an adjuvant at 0, 2, and 4 weeks. Four days after the final immunization the mice were euthanized, their spleens were harvested, and a fusion was performed in accordance with standard methodology (40). Hybridomas that reacted to proteinase K-resistant, periodate-sensitive bacterial surface epitopes were selected for further analyses. MAb 13D6 met these criteria and was shown to be directed against the K1 capsule (31). Isotyping (Zymed Laboratories Inc.; mouse MonoAb-ID kit) established that MAb 13D6 was an IgM. The MAb 13D6 hybridoma was sent to Maine Biotechnology Services for production of purified MAb. The harvested ascites fluid had a total protein concentration of 34.92 mg/ml, 8.08% of which was immunoglobulin, resulting in an estimated 2.8 mg/ml of MAb 13D6. Since it is possible that background antibodies may be present in the ascites fluid, the actual concentration of MAb 13D6 may be lower. This preparation was used for *in vitro* and *in vivo* studies.

**Generation of polyclonal K1 antisera.** Capsular polysaccharide was extracted with cold 0.1 M pyridine acetate (pH 5.0) as described previously (41). The extract was dialyzed against endotoxin-free water and then treated with proteinase K, DNase I, and RNase A. Preimmunization antisera were obtained, and CD1 outbred male mice (18 to 20 g) were intramuscularly immunized with capsule purified from 150 mg (wet weight) of bacteria ($n = 6$) or with 1× phosphate-buffered saline (PBS) (pH 7.2) ($n = 6$) without adjuvant at 0, 2, and 4 weeks to generate anti-K1 immune and nonimmune antisera, respectively. Anti-K1 immune antisera, obtained at 5 weeks after initial immunization, were pooled and absorbed against AB307.30 (isogenic K1-negative derivative of AB307-0294) to remove any noncapsular antibodies that may have been generated from the presence of trace contaminants in the capsule preparation used for immunization. An immune dot assay was used to quantitate the immunogenicity of the K1 capsule. Preimmune and nonimmune antisera were nonreactive at the lowest dilution of 1:250. Anti-K1 immune antisera were reactive at a 1/25,000 dilution. These preparations were used to assess the anti-capsule IgG/IgM response via flow cytometry by comparing serum reactivities between the wild-type strain AB307-0294 and AB307.30, the difference reflecting anticapsular antibody.

**Flow cytometry studies for the detection of polyclonal K1 antisera reactivity to AB307-0294 (K1 capsule positive) and AB307.30 (K1 capsule negative).** Flow-cytometric assessment of antibody binding was performed as described previously (42). In brief, the appropriate strains were grown in LB medium, diluted to $1 \times 10^6$ CFU, washed in 100 μl of 1× PBS, resuspended in 100 μl of 1:100-diluted preimmune, nonimmune, or anti-K1 immune polyclonal mouse antiserum (complement inactivated by heating at 56°C for 30 min), and incubated for 60 min at 37°C with constant rotation. Preliminary experiments established that this incubation time and dilution resulted in maximal antibody binding (data not shown). Following incubation the bacteria were washed once with 0.5 ml of 1× PBS, resuspended in 100 μl of goat anti-mouse IgG/IgM–fluorescein isothiocyanate (FITC)-labeled conjugate (Caltag Laboratories), and incubated at 37°C for 30 min with constant rotation. Bacteria were washed, resuspended in 500 μl of 1× PBS, transferred to 5-ml tubes, and assayed for antibody binding by flow cytometry. Ten thousand bacterial events were gated in the forward-scatter versus side-scatter plot, discriminating them from "debris," and antibody-bound-bacterium events were assessed in the FL-1 channel and reported as percent positives or geometric mean fluorescence (GMF). Binding in the presence of the FITC-labeled conjugate alone served as the nonspecific binding control. An autofluorescence control consisted of bacteria incubated in the absence of antibody.

**Colony lift immunoassays.** Numbered grids were marked on the back of LB plates. Bacterial strains were assigned a number, streaked onto the designated grid, and incubated overnight at 37°C. The next day a nitrocellulose transfer membrane that was marked for orientation was placed onto the colonies, incubated at 4°C for 15 min, and then carefully removed and dried at 37°C for 1 h. The membrane was washed with Tris-buffered saline (10 mM Tris, 150 mM NaCl, pH 7.4; TBS) to remove excess bacteria, blocked while being shaken with 3% nonfat milk in TBS for 1 h at room temperature, washed again with TBS, and then incubated overnight while being shaken at 4°C with MAb 13D6 (undiluted culture supernatants). After overnight incubation, the membrane was washed with TBS and incubated for 1 h at room temperature with a 1/3,000 dilution of peroxidase-labeled goat anti-mouse IgM (μ) antibody (KPL). Subsequently the membrane was washed with TBS and developed with 4-chloro-1-naphthol (Sigma) in methanol-TBS-$H_2O_2$ until the desired color development. Reactions were stopped with distilled water.

**PMN-mediated bactericidal assay.** A neutrophil (PMN)-mediated bactericidal assay was performed essentially as described previously (43). For these studies MAb 13D6 (specific for the K1 capsule) or MAb3F7 (IgM isotype control specific for the *Moraxella catarrhalis* serotype B lipooligosaccharide [LOS] [44]) was used. In brief, $1.0 \times 10^6$ CFU of AB307-0294 (K1 capsule positive), AB307.30 (homologous capsule negative), AB797 (heterologous K1 negative), AB693 (heterologous K1 capsule positive), AB715 (heterologous K1 capsule positive), and AB803 (heterologous K1 capsule positive) were either (i) preopsonized for 50 min at 37°C in 90 μl of 1× PBS (pH 7.4) plus 10 μl of MAb (final 1:10 dilution; previously heated at 56°C for 30 min to inactivate complement [Δ56°C]) or (ii) incubated for 50 min at 37°C with 100 μl of 1× PBS in the absence of MAb. After incubation, bacteria were brought to a volume of 5 ml by adding 20% Δ56°C plasma–1× PBS (pH 7.4) (plasma-PBS), resulting in an estimated $2 \times 10^5$ CFU/ml of AB307-0294 (quantified by a subsequent titer). Five hundred microliters of opsonized or nonopsonized AB307-0294 was added to each well of a tissue culture plate (Costar 3472-clear; Corning Inc., Corning, NY) that contained either $5 \times 10^5$ human PMNs purified via a Ficoll-Hypaque gradient (Amersham) (45) in 500 μl of plasma-PBS (PMNs were allowed to adhere at room temperature for 30 min) or 500 μl of plasma-PBS alone. To expedite contact between bacteria and neutrophils, the tissue culture plate was spun at 218 × *g* for 10 min and placed at 37°C in a $CO_2$ incubator. After 60 min, 20 μl of saponin (from a 25-mg/ml stock solution in $H_2O$) was added to each well and the titer of AB307-0294 was determined. Bacterial titers were calculated as the initial log CFU minus the log CFU after 1 h of incubation at 37°C for the following conditions: (i) no antibody/PMN negative, (ii) no antibody/PMN positive, (iii) antibody/PMN negative, and (iv) antibody/PMN positive. The metric of interest for this assay was the difference between bacterial titers in the presence of PMN with or without MAb (condition ii versus iv), which reflects the effect of opsonization.

**Rat soft tissue infection model.** An established rat (Long-Evans) soft tissue infection model was employed as previously reported (34). The rat soft tissue infection model studies were reviewed and approved by the University at Buffalo and Veterans Administration Institutional Animal Care Committee. In brief, a subcutaneous pouch was created through the injection of 30 ml of air into the back of anesthetized male Long-Evans rats (175 to 200 g), followed by the injection of 1 ml of 1% croton oil in a filter-sterilized vegetable oil vehicle. The space is allowed to mature into an encapsulated, fluid-filled (8- to 12-ml) "pouch" over 6 to 8 days. AB307-0294 and AB979 were injected into the pouch to achieve starting titers of approximately $1 \times 10^5$ and $1 \times 10^3$ CFU/ml, respectively. In this manner, due to various *in vivo* growth characteristics, the bacterial titers in the pouch would be similar at the time of initial treatment with the K1 capsule-specific MAb 13D6. Pouch fluid was removed to enumerate bacterial counts at 1 min, 3 h, 6 h, 24 h, and 48 h postinoculation. For passive immunization studies, animals were treated via injection into the pouch with 2.35 mg of the K1 capsule-specific MAb 13D6 or a 1× PBS control at 3 and 24 h after bacterial challenge.

**Statistical analyses.** Continuous data were assessed for normality and presented as means ± standard errors of the means (SEM). *P* values of $0.05/n$ ($n$ = the number of comparisons) are considered statistically significant based on the Bonferroni correction for multiple comparisons. A statistical trend was defined as a *P* value $<0.1/n$ but $>0.05/n$. *In vivo* activity of MAb 13D6 was defined as a difference in the survival and growth of the test strain in animals treated with MAb 13D6 compared to those in animals treated with buffer alone. To normalize *in vitro* and *in vivo* data, $\log_{10}$-transformed values were utilized, the area under each curve was calculated, and these areas were compared using two-tailed unpaired *t* tests (Prism 4 for MacIntosh; GraphPad Software Inc.).

## RESULTS

**The structure of the K1 capsule.** CE-ES-MS and NMR spectroscopy structural analyses indicated that a high-molecular-weight polysaccharide polymer, consistent with capsular polysaccharide, could be identified from the AB307-0294, but not the AB307.30, polysaccharide preparations. Structural elucidations were performed on the purified high-molecular-weight polymer isolated following anion-exchange chromatography. Mass spectrometric analysis suggested that the polymer was made up of a trisaccharide repeat unit with residues of masses of 203, 217, and 228 Da. There was also evidence of an alternate trisaccharide made up of residues with masses of 203, 217, and 272 Da (Fig. 1). NMR analysis confirmed and extended this observation, revealing that the polymer was identical to that identified previously from *A. baumannii* strain 24 (46), with a trisaccharide repeat unit consisting of three residues, all in pyranose form: α-galactosaminuronic acid (A), α-*N*-acetylglucosamine (B), and 2,4-diamino-2,4,6-trideoxy-glucose (bacillosamine; C). The capsule structure is as follows: -[3-β-D-QuiNAc4NR-1-4-α-GlcNAc6OAc-1-4-α-D-GalNAcA-1-]$_n$-, where residue A is 4-α-D-GalNAcA-1, residue B is 4-α-GlcNAc6OAc-1, and residue C is 3-β-D-QuiNAc4NR-1. The O-acetylation on residue B is present in approximately 70% of the repeat units, and for residue C the amino group at the 4 position is modified such that R is either an acetyl or a 3-OH-butyrate group in an approximately 1:1 ratio. These data also demonstrate that the K1 capsule is distinct from the AB307-0294 lipopolysaccharide (47) and the extracellular polysaccharide poly-β-(1-6)-*N*-acetylglucosamine (48).

**The K1 capsule is not predicted to be cross-reactive to human epitopes.** The *A. baumannii* capsule might induce antibodies that are reactive to human epitopes, which would be a risk factor for the development of autoimmune disease. Importantly, structural data (see above; Fig. 1) did not identify any known cross-reactive epitopes, such as sialic acid. The K1 capsule does contain bacillosamine, a rare amino sugar, which is not present in humans (49).

**The K1 capsule is immunogenic.** A mandatory trait for a vaccine candidate is immunogenicity. Although the overwhelming majority of capsular serotypes are very immunogenic, some are poor immunogens (e.g., the polysialic acid K1 capsule from extraintestinal pathogenic *Escherichia coli*) (50, 51). Therefore, the immunogenicity of the *A. baumannii* K1 capsule was assessed by intramuscular injection of CD1 mice with purified capsule or with 1× PBS without adjuvant at 0, 2, and 4 weeks to generate anti-K1 immune or nonimmune antisera, respectively. Antisera, obtained at 5 weeks after the initial immunization, were used to assess the immune response against capsule by flow cytometry. These data clearly established that the K1 capsule was immunogenic (Table 1 and Fig. 2; both generated from the same data set). This was dem-

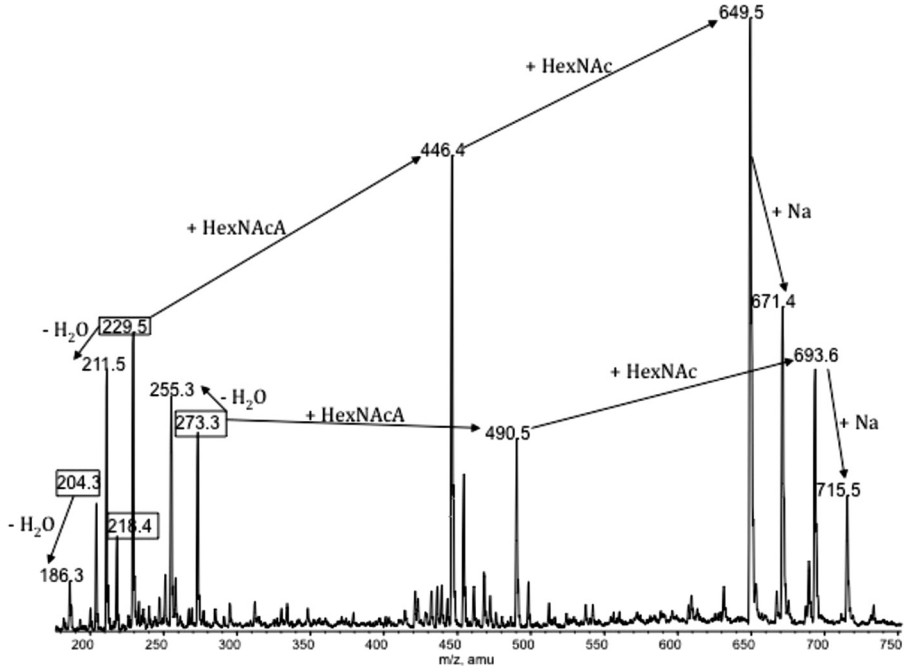


**FIG 1** Positive-ion CE-ES-MS of purified capsular polysaccharide from AB307-0294. Boxed ions refer to $HexNAc^+$ (204 Da), $HexNAcA^+$ (218 Da), 6-dHexNAc4NAc$^+$ (229 Da), and 6-dHexNAc4NBu$^+$ (273 Da). Addition of HexNAc and HexNAcA to these residues is indicated with arrows, as are anhydro glycoforms ($-H_2O$) and sodiated glycoforms ($+Na$).

onstrated by the significant increase in reactivity observed with the anti-K1 immune serum against AB307-0294 (K1 capsule positive) compared to that observed with AB307.30 (K1 capsule negative) ($P < 0.05$).

**Thirteen percent of *A. baumannii* strains studied possess the K1 serotype.** Colony lift immunoasays were used to assess the seroprevalence of the K1 serotype in a collection of 100 *A. baumannii* strains. The ST, geographic origin, and site of isolation for all stains, when known, are listed in Table S1 in the supplemental material. The overall seroprevalence of K1-positive strains was 13%. The sites of isolation for the K1-positive strains were blood ($n = 6$), axilla ($n = 2$), wounds ($n = 1$), urine ($n = 1$), environment ($n = 1$), and unknown ($n = 2$). The known STs for the K1-positive strains were ST14 ($n = 6$), ST15 ($n = 1$), and ST16 ($n = 1$). All ST14 strains were K1 positive, but the collection contained 3 ST15 strains and one ST16 strain that were K1 negative.

**TABLE 1** Binding of anti-K1 immune and nonimmune polyclonal mouse antisera to AB307-0294 (K1 capsule positive) and AB307.30 (K1 capsule negative) as assessed by flow cytometry

| Parameter | Value[a] for: | |
|---|---|---|
| | AB307-0294 | AB307.30 |
| % bacterial cells bound with: | | |
| Nonimmune antisera | 2.2 ± 0.2 | 1.2 ± 0.1 |
| Anti-K1 immune antisera | 84.9 ± 1.9* | 6.3 ± 0.4 |
| Geometric mean fluorescence of cells bound with: | | |
| Nonimmune antisera | 2.8 ± 0.02 | 5.8 ± 0.2 |
| Anti-K1 immune antisera | 137.3 ± 12* | 8.6 ± 0.2 |

[a] *, $P < 0.05$ (*t* test) for AB307-0294 compared to AB307.30. Values are means ± SEM for $n = 3$ or 4.

**MAb 13D6 increases neutrophil-mediated bactericidal activity *in vitro*.** An *in vitro* neutrophil opsonophagocytosis assay was performed to assess whether opsonization of K1-positive strains with MAb 13D6 increased bactericidal activity. The bactericidal activity of interest was reflected by the initial log CFU minus the log CFU after 1 h of incubation at 37°C in the presence of human PMNs with and without opsonization.

Opsonization with MAb 13D6 significantly increased bactericidal activity against the K1-positive strains AB307-0294, AB693, and AB803 ($P < 0.05$), and there was a trend for AB715 ($P = 0.0596$) compared to nonopsonized bacteria (Fig. 3A and D to F). By contrast, opsonization with MAb 13D6 did not significantly increase bactericidal activity against the K1-negative strains AB307.30 and AB797 compared to nonopsonized bacteria (Fig. 3B and C). Opsonization with MAb3F7, an isotype control, did not significantly increase bactericidal activity against any of the strains (data not shown). Taken together, these data demonstrate that the increased neutrophil-mediated bactericidal activity against K1-positive strains observed in the presence of MAb 13D6 is a specific effect and support the potential therapeutic utility of antibodies directed against the K1 capsule for K1-positive strains.

**Passive immunization with MAb 13D6 increases clearance of the K1-positive strain AB307-0294.** To test the hypothesis that passive immunization could be used therapeutically for infections due to *A. baumannii*, an established rat soft tissue infection model was used (34). This model is clinically relevant since *A. baumannii* has been recognized as a cause of a variety of soft tissue infections (6, 7). In this model a subcutaneous encapsulated, fluid-filled "pouch" was created, from which multiple fluid samplings after bacterial challenge were obtained in order to enumerate CFU. AB307-0294 (K1 positive) and AB979 (K1 negative) were injected into the pouch so that, when treatment with MAb 13D6 occurred

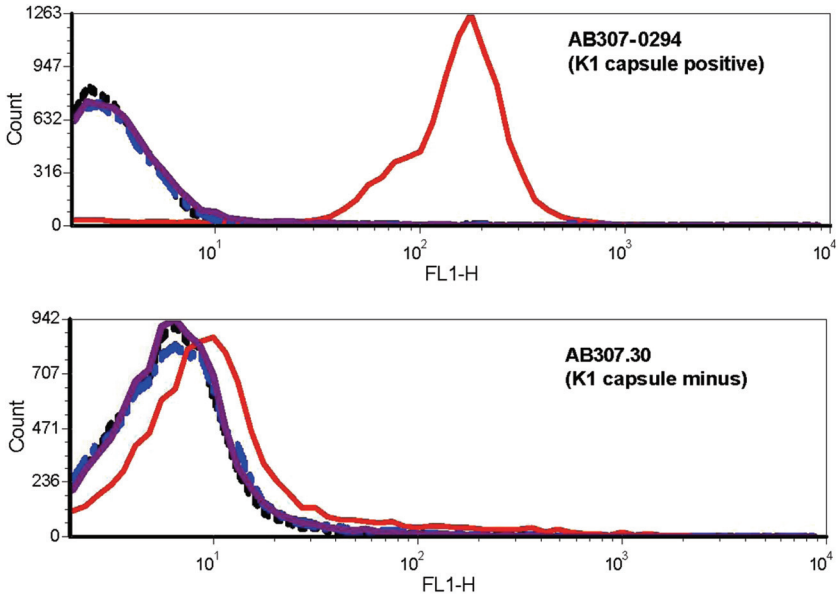


**FIG 2** The K1 capsule present on AB307-0294 is immunogenic. Binding of preimmune, nonimmune, and anti-K1 immune polyclonal mouse antisera to AB307-0294 (wild type; K1 capsule positive) and AB307.30 (K1 capsule minus) was detected by goat anti-mouse IgG/IgM–fluorescein isothiocyanate (FITC)-labeled conjugate. Preimmune serum was obtained from animals prior to immunization (negative control). Nonimmune antiserum was generated by immunizing CD1 mice with 1× PBS alone (negative control). Anti-K1 immune antiserum was generated by immunizing mice with extracted K1 capsule from AB307-0294, followed by subsequent absorption against the capsule-negative derivative AB307.30. Representative curves are shown. Preimmune antiserum, black dashed lines; nonimmune antiserum, solid purple lines; anti-K1 immune antiserum, solid red lines; FITC-labeled conjugate alone (nonspecific binding control), blue dashed lines. An autofluorescence control (antibody not added) was also performed, and the curves were similar to the other negative controls (data not shown).

3 h after bacterial challenge, their titers would be similar. A second treatment with MAb 13D6 was given at 24 h (Fig. 4, arrows). Treatment with MAb 13D6 significantly decreased the growth/survival of AB307-0294 compared to treatment with 1× PBS ($P < 0.05$) (Fig. 4A). By contrast, AB979 was unaffected by treatment with MAb 13D6 (Fig. 4B). These data support the concept that treatment of infection due to *A. baumannii* with antibodies directed against capsular polysaccharide has therapeutic potential.

## DISCUSSION

Given the paucity of new antimicrobial agents active against GNB in the pharmaceutical pipeline (19, 20), consideration of passive immunization as a treatment modality is warranted. In this report, we tested the hypothesis that antibodies directed against a capsular polysaccharide of *A. baumannii* have therapeutic potential via passive immunization. Previous work established that the K1 capsular polysaccharide from the *A. baumannii* strain AB307-0294 is surface exposed and is a virulence factor (31). Data reported here extend these observations. The K1 capsule is immunogenic (Table 1 and Fig. 2). Opsonization of the K1-positive strain AB307-0294 with MAb 13D6, which is directed against the K1 capsule, increases neutrophil-mediated bactericidal activity *in vitro* (Fig. 3). Lastly, treatment after the initiation of infection with MAb 13D6 increases bacterial clearance in an *in vivo* soft tissue infection model (Fig. 4). While previous studies have shown that bacterial capsules can be effective immunogens, this is the first set of data to our knowledge that supports the potential use of the capsular polysaccharide as a target for antibody-mediated therapeutics in *A. baumannii*. Additional targets which may also be useful include OmpA (23) and the noncapsular bacterial surface polysaccharide poly-β-(1-6)-*N*-acetylglucosamine (52).

Active or passive immunization raises the concern for an autoimmune response. Selected lipooligosaccharide (LOS) serotypes of *Campylobacter jejuni* that contain *N*-acetylneuraminic acid (sialic acid) are mimics of human gangliosides and have been associated with development of Guillain-Barre and the Miller Fisher variant (53, 54). The *N. meningitidis* serogroup B capsule and the *E. coli* K1 capsule are polysialic acid capsules that are potential mimics of host tissue. The neisserial serogroup B capsule can induce antibodies that are cross-reactive with the embryonic but not adult neural cell adhesion molecules (55). Further, certain *Neisseria* and *Haemophilus* LOS structures mimic glycosphingolipids and gangliosides; however, evidence that antibodies directed against these structures cause autoimmune disease in humans is not compelling (56). The delineation of the K1 capsule did not identify any mimics, such as sialic acid, of concern for cross-reactivity to human epitopes (Fig. 1). Nonetheless, formal testing would be required to support the speculation that this immunogen could be safely used in humans.

A potential limitation for the use of capsule as a target for passive or active immunization would be the existence of a large number of clinically relevant serotypes. For example, more than 80 capsular serotypes exist for *E. coli* strains (57, 58). It is not known how many capsular serotypes exist for *A. baumannii*. However, the initial seroprevalence data on K1 (13% of the strains studied) are encouraging. We appreciate that a greater and more geographically diverse number of clinical isolates require serotyping to more definitively define K1 seroprevalence. However, since K1-positive strains comprised 13% of the *A. baumannii* strains tested, this suggests that the number of capsular serotypes in *A. baumannii* may not be overwhelming. From an active-vaccination

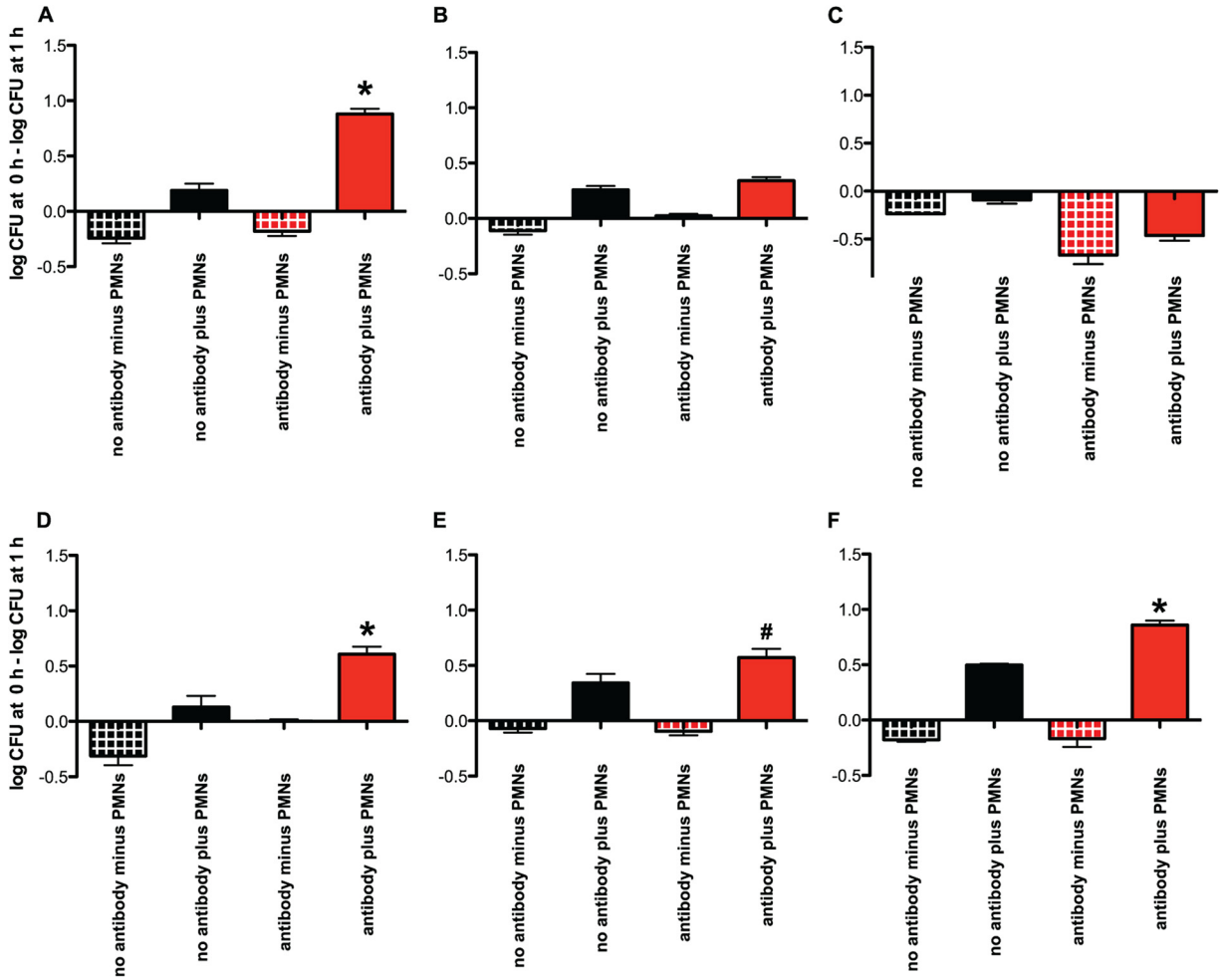


**FIG 3** Opsonization with MAb 13D6 significantly increases neutrophil (PMN)-mediated bactericidal activity *in vitro* against K1-positive, but not K1-negative strains. Neutrophil-mediated bactericidal activity against opsonized (with MAb 13D6) and nonopsonized *A. baumannii* strains in the presence or absence of PMN is shown. The opsonophagocytosis assay was performed as described in Materials and Methods. (A) AB307-0294 (homologous K1 positive); (B) AB307.30 (homologous K1 negative); (C) AB797 (heterologous K1 negative); (D) AB693 (heterologous K1 positive); (E) AB715 (heterologous K1 positive); (F) AB803 (heterologous K1 positive). $n = 3$ to 6. *, $P < 0.05$; #, $P < 0.1$ but $> 0.05$ (two-tailed unpaired $t$ test).

perspective, identification of 10 to 20 clinically important capsular serotypes would be encouraging since 13-valent conjugated and 23-valent nonconjugated capsular polysaccharide vaccines are already in clinical use for prevention of *S. pneumoniae* infections.

The use of anticapsular antisera as a treatment modality (passive immunization) presents a greater number of challenges. First, it would likely only be considered in the setting of defined infections caused by extremely resistant or panresistant *A. baumannii*.

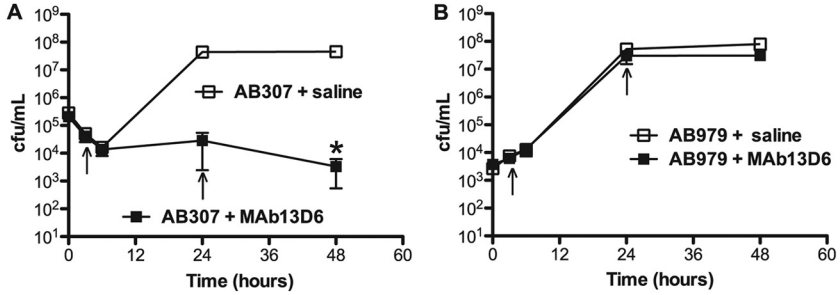


**FIG 4** Passive immunization with MAb 13D6 significantly increases the *in vivo* clearance of AB307-0294 (K1 positive) but not AB979 (K1 negative). Growth/survival of *A. baumannii* strains AB307-0294 (A) and AB979 (B) in the rat soft tissue infection model with or without treatment with MAb 13D6 is shown. Details are in Materials and Methods. At 3 and 24 h after bacterial challenge the infected pouches were treated with the K1 capsule-specific MAb 13D6 or 1× PBS (arrows). AB307-0294 and AB979 were injected into the pouch to achieve bacterial titers that would be similar at the time of initial treatment with MAb 13D6. Data are means ± SEM ($n = 8$ for AB307-0294 and $n = 4$ for AB979). *, $P < 0.05$ for AB307-0294 treated with MAb 13D6 compared to AB307-0294 treated with 1× PBS.

Further, the commercial development of multiple capsule serotype-specific antisera would be needed. Another limitation would be the need for laboratory identification of the serotype, but this could be easily accomplished via a rapid immunologic or PCR-based approach. Serotype-specific capsular antisera for passive immunization would likely be optimal due to both cost and potential efficacy (concentration related) considerations. However, despite these potential challenges, unless new classes of antimicrobials active against extremely resistant or panresistant *A. baumannii* are developed, this alternative approach warrants consideration.

We demonstrated that MAb 13D6, which is directed against the K1 capsule, increased neutrophil-mediated bactericidal activity *in vitro* and could be used to increase the clearance of the K1-positive strain AB307-0294 in a soft tissue infection model. The lack of an effect of MAb 13D6 on the *in vivo* growth and/or survival of AB979, which has a non-K1 capsule, established specificity. It might seem logical to have used the isogenic K1-negative derivative AB307.30 instead of AB979 for these studies. Unfortunately this was not possible because AB307.30 is readily cleared in this infection model, likely due to an increased sensitivity to complement-mediated bactericidal activity (31). The goal of this set of studies was to establish capsule as a potential therapeutic target via passive immunization. We appreciate that MAb 13D6 may not optimize clearance of K1 *A. baumannii* strains. The development of alternative antibodies with enhanced affinity and/or an alternative isotype would likely confer an even greater degree of efficacy. We also appreciate that the efficacy of passive immunization as a treatment modality needs to be assessed in other infection models. However, the fact that we were able to achieve a 4-log decrease in bacterial CFU compared to no treatment in a model of closed-space infections, which are notoriously difficult to cure in the absence of drainage, is encouraging and establishes proof of principle. A strength of this study was that animals were treated with MAb 13D6 after infection was established. Pretreatment or simultaneous treatment at the time of bacterial challenge is a far less rigorous approach for establishing efficacy and is clinically less relevant. Further, the use of passive immunization to prevent *A. baumannii* infection would be impractical.

In summary, data are presented that support the proof of principle that the *A. baumannii* K1 capsular polysaccharide is a viable therapeutic target via passive immunization. Future studies will need to establish the number and prevalence of non-K1 capsular polysaccharides from *A. baumannii* and determine whether these serotypes are also amenable to an antibody-based therapeutic intervention.

## ACKNOWLEDGMENTS

This work was supported in part by a VA Merit Review from the Department of Veterans Affairs (T.A.R.), by a Telemedicine and Advance Technical Research Center Cooperative Agreement W23RYX1055N607 (T.A.R.), and by National Institutes of Health grants 1R21AI088318-01A1 (T.A.R.) and 1R21 AI101426-01 (A.A.C.).

The funders had no role in study design, data collection and analysis, decision to publish, or preparation of the manuscript.

We thank Jacek Stupak for mass spectrometry and Bruce Davidson for assistance in analyzing flow cytometry data.

## REFERENCES

1. **Perez F, Endimiani A, Bonomo RA.** 2008. Why are we afraid of Acinetobacter baumannii? Expert Rev. Anti Infect. Ther. **6**:269–271.
2. **Perez F, Hujer AM, Hujer KM, Decker BK, Rather PN, Bonomo RA.** 2007.Global challenge of multidrug-resistant Acinetobacter baumannii. Antimicrob. Agents Chemother. **51**:3471–3484.
3. **Fournier PE, Richet H.** 2006.The epidemiology and control of Acinetobacter baumannii in health care facilities. Clin. Infect. Dis. **42**:692–699.
4. **van Dessel H, Kamp-Hopmans TE, Fluit AC, Brisse S, de Smet AM, Dijkshoorn L, Troelstra A, Verhoef J, Mascini EM.** 2002. Outbreak of a susceptible strain of Acinetobacter species 13 (sensu Tjernberg and Ursing) in an adult neurosurgical intensive care unit. J. Hosp. Infect. **51**:89–95.
5. **Richet H, Fournier PE.** 2006. Nosocomial infections caused by Acinetobacter baumannii: a major threat worldwide. Infect. Control Hosp. Epidemiol. **27**:645–646.
6. **Falagas ME, Karveli EA.** 2007. The changing global epidemiology of Acinetobacter baumannii infections: a development with major public health implications. Clin. Microbiol. Infect. **13**:117–119.
7. **Peleg AY, Seifert H, Paterson DL.** 2008. Acinetobacter baumannii: emergence of a successful pathogen. Clin. Microbiol. Rev. **21**:538–582.
8. **Anstey NM, Currie BJ, Hassell M, Palmer D, Dwyer B, Seifert H.** 2002. Community-acquired bacteremic Acinetobacter pneumonia in tropical Australia is caused by diverse strains of Acinetobacter baumannii, with carriage in the throat in at-risk groups. J. Clin. Microbiol. **40**:685–686.
9. **Anstey NM, Currie BJ, Withnall KM.** 1992. Community-acquired Acinetobacter pneumonia in the Northern Territory of Australia. Clin. Infect. Dis. **14**:83–91.
10. **Chen MZ, Hsueh PR, Lee LN, Yu CJ, Yang PC, Luh KT.** 2001. Severe community-acquired pneumonia due to Acinetobacter baumannii. Chest **120**:1072–1077.
11. **Garzoni C, Emonet S, Legout L, Benedict R, Hoffmeyer P, Bernard L, Garbino J.** 2005. Atypical infections in tsunami survivors. Emerg. Infect. Dis. **11**:1591–1593.
12. **Maegele M, Gregor S, Steinhausen E, Bouillon B, Heiss MM, Perbix W, Wappler F, Rixen D, Geisen J, Berger-Schreck B, Schwarz R.** 2005. The long-distance tertiary air transfer and care of tsunami victims: injury pattern and microbiological and psychological aspects. Crit. Care Med. **33**:1136–1140.
13. **Gaynes R, Edwards JR.** 2005. Overview of nosocomial infections caused by gram-negative bacilli. Clin. Infect. Dis. **41**:848–854.
14. **Roca I, Espinal P, Vila-Farres X, Vila J.** 2012. The Acinetobacter baumannii oxymoron: commensal hospital dweller turned pan-drug-resistant menace. Front. Microbiol. **3**:148.
15. **Fishbain J, Peleg AY.** 2010. Treatment of Acinetobacter infections. Clin. Infect. Dis. **51**:79–84.
16. **Magiorakos AP, Srinivasan A, Carey RB, Carmeli Y, Falagas ME, Giske CG, Harbarth S, Hindler JF, Kahlmeter G, Olsson-Liljequist B, Paterson DL, Rice LB, Stelling J, Struelens MJ, Vatopoulos A, Weber JT, Monnet DL.** 2012. Multidrug-resistant, extensively drug-resistant and pandrug-resistant bacteria: an international expert proposal for interim standard definitions for acquired resistance. Clin. Microbiol. Infect. **18**:268–281.
17. **Howard A, O'Donoghue M, Feeney A, Sleator RD.** 2012. Acinetobacter baumannii: an emerging opportunistic pathogen. Virulence. **3**:243–250.
18. **Boucher HW, Talbot GH, Bradley JS, Edwards JE, Gilbert D, Rice LB, Scheld M, Spellberg B, Bartlett J.** 2009. Bad bugs, no drugs: no ESKAPE! An update from the Infectious Diseases Society of America. Clin. Infect. Dis. **48**:1–12.
19. **Boucher, H., Gilbert D, Benjamin D, Bradley J., Murray B, Spellberg B, Talbot G.** 2011. 10 x '20 progress: development of new drugs active against resistant Gram-negative bacilli, abstr. LB-27. Abstr. 49th Annu. Meet. Infect. Dis. Soc. Am., Boston, MA.
20. **Butler MS, Cooper MA.** 2011. Antibiotics in the clinical pipeline in 2011. J. Antibiot. **64**:413–425.
21. **Hsu JL, Safdar N.** 2011. Polyclonal immunoglobulins and hyperimmune globulins in prevention and management of infectious diseases. Infect. Dis. Clin. North Am. **25**:773–788.
22. **Both L, Banyard AC, van Dolleweerd C, Horton DL, Ma JK, Fooks AR.** 2012. Passive immunity in the prevention of rabies. Lancet Infect. Dis. **12**:397–407.
23. **Luo G, Lin L, Ibrahim AS, Baquir B, Pantapalangkoor P, Bonomo RA, Doi Y, Adams MD, Russo TA, Spellberg B.** 2012. Active and passive immunization protects against lethal, extreme drug resistant-Acinetobacter baumannii infection. PLoS One **7**:e29446. doi:10.1371/journal.pone.0029446.

24. **Fedson DS, Nicolas-Spony L, Klemets P, van der Linden M, Marques A, Salleras L, Samson SI.** 2011. Pneumococcal polysaccharide vaccination for adults: new perspectives for Europe. Expert Rev. Vaccines **10**:1143–1167.
25. **O'Loughlin RE, Edmond K, Mangtani P, Cohen AL, Shetty S, Hajjeh R, Mulholland K.** 2010. Methodology and measurement of the effectiveness of Haemophilus influenzae type b vaccine: systematic review. Vaccine **28**:6128–6136.
26. **Safadi MA, McIntosh ED.** 2011. Epidemiology and prevention of meningococcal disease: a critical appraisal of vaccine policies. Expert Rev. Vaccines **10**:1717–1730.
27. **Bryant KA, Marshall GS.** 2011. Haemophilus influenzae type b-Neisseria meningitidis serogroups C and Y tetanus toxoid conjugate vaccine for infants and toddlers. Expert Rev. Vaccines **10**:941–950.
28. **Engels EA, Lau J.** 2000. Vaccines for preventing typhoid fever. Cochrane Database Syst. Rev. CD001261. doi:10.1002/14651858.CD001261.
29. **Avci FY, Kasper DL.** 2010. How bacterial carbohydrates influence the adaptive immune system. Annu. Rev. Immunol. **28**:107–130.
30. **Blanchard-Rohner G, Pollard AJ.** 2011. Long-term protection after immunization with protein-polysaccharide conjugate vaccines in infancy. Expert Rev. Vaccines **10**:673–684.
31. **Russo TA, Luke NR, Beanan JM, Olson R, Sauberan SL, MacDonald U, Schultz LW, Umland TC, Campagnari AA.** 2010. The K1 capsular polysaccharide of Acinetobacter baumannii strain 307-0294 is a major virulence factor. Infect. Immun. **78**:3993–4000.
32. **Ecker JA, Massire C, Hall TA, Ranken R, Pennella TT, Agasino Ivy C, Blyn LB, Hofstadler SA, Endy TP, Scott PT, Lindler L, Hamilton T, Gaddy C, Snow K, Pe M, Fishbain J, Craft D, Deye G, Riddell S, Milstrey E, Petruccelli B, Brisse S, Harpin V, Schink A, Ecker DJ, Sampath R, Eshoo MW.** 2006. Identification of Acinetobacter species and genotyping of Acinetobacter baumannii by multilocus PCR and mass spectrometry. J. Clin. Microbiol. **44**:2921–2932.
33. **Russo TA, MacDonald U, Beanan JM, Olson R, MacDonald IJ, Sauberan SL, Luke NR, Schultz LW, Umland TC.** 2009. Penicillin-binding protein 7/8 contributes to the survival of Acinetobacter baumannii in vitro and in vivo. J. Infect. Dis. **199**:513–521.
34. **Russo TA, Beanan JM, Olson R, MacDonald U, Luke NR, Gill SR, Campagnari AA.** 2008. Rat pneumonia and soft-tissue infection models for the study of Acinetobacter baumannii biology. Infect. Immun. **76**:3577–3586.
35. **Westphal O, Jann K.** 1965. Bacterial lipopolysaccharide. Methods Carbohydr. Chem. **5**:88–91.
36. **Vinogradov EV, Van Der Drift K, Thomas-Oates JE, Meshkov S, Brade H, Holst O.** 1999. The structures of the carbohydrate backbones of the lipopolysaccharides from Escherichia coli rough mutants F470 (R1 core type) and F576 (R2 core type). Eur. J. Biochem. **261**:629–639.
37. **St Michael F, Li J, Vinogradov E, Larocque S, Harper M, Cox AD.** 2005. Structural analysis of the lipopolysaccharide of Pasteurella multocida strain VP161: identification of both Kdo-P and Kdo-Kdo species in the lipopolysaccharide. Carbohydr. Res. **340**:59–68.
38. **Campagnari AA, Ducey TF, Rebmann CA.** 1996. Outer membrane protein B1, an iron-repressible protein conserved in the outer membrane of Moraxella (Branhamella) catarrhalis, binds human transferrin. Infect. Immun. **64**:3920–3924.
39. **Loehfelm TW, Luke NR, Campagnari AA.** 2008. Identification and characterization of an Acinetobacter baumannii biofilm-associated protein. J. Bacteriol. **190**:1036–1044.
40. **Haase EM, Campagnari AA, Sarwar J, Shero M, Wirth M, Cumming CU, Murphy TF.** 1991. Strain-specific and immunodominant surface epitopes of the P2 porin protein of nontypeable Haemophilus influenzae. Infect. Immun. **59**:1278–1284.
41. **Russo T, Guenther J, Wenderoth S, Frank M.** 1993. Generation of isogenic K54 capsule-deficient *Escherichia coli* strains through Tn*phoA*-mediated gene disruption. Mol. Microbiol. **9**:357–364.
42. **Russo TA, Beanan JM, Olson R, Genagon SA, Macdonald U, Cope JJ, Davidson BA, Johnston B, Johnson JR.** 2007. A killed, genetically engineered derivative of a wild-type extraintestinal pathogenic E. coli strain is a vaccine candidate. Vaccine **25**:3859–3870.
43. **Russo TA, Beanan JM, Olson R, Macdonald U, Cope JJ.** 2009. Capsular polysaccharide and the O-specific antigen impede antibody binding: a potential obstacle for the successful development of an extraintestinal pathogenic Escherichia coli vaccine. Vaccine **27**:388–395.
44. **Edwards KJ, Allen S, Gibson BW, Campagnari AA.** 2005. Characterization of a cluster of three glycosyltransferase enzymes essential for Moraxella catarrhalis lipooligosaccharide assembly. J. Bacteriol. **187**:2939–2947.
45. **Russo, TA, Davidson BA,, Genagon SA, Warholic NM, Macdonald U, Pawlicki PD, Beanan JM, Olson R, Holm BA, Knight PR, III.** 2005. E. coli virulence factor hemolysin induces neutrophil apoptosis and necrosis/lysis in vitro and necrosis/lysis and lung injury in a rat pneumonia model. Am. J. Physiol. Lung Cell. Mol. Physiol. **289**:L207–L216.
46. **Vinogradov EV, Brade L, Brade H, Holst O.** 2003. Structural and serological characterisation of the O-antigenic polysaccharide of the lipopolysaccharide from Acinetobacter baumannii strain 24. Carbohydr. Res. **338**:2751–2756.
47. **Luke NR, Sauberan SL, Russo TA, Beanan JM, Olson R, Loehfelm TW, Cox AD, St. Michael F, Vinogradov EV, Campagnari AA.** 2010. Identification and characterization of a glycosyltransferase involved in Acinetobacter baumannii lipopolysaccharide core biosynthesis. Infect. Immun. **78**:2017–2023.
48. **Choi AH, Slamti L, Avci FY, Pier GB, Maira-Litran T.** 2009. The pgaABCD locus of Acinetobacter baumannii encodes the production of poly-beta-1-6-N-acetylglucosamine, which is critical for biofilm formation. J. Bacteriol. **191**:5953–5963.
49. **Sharon N.** 2007. Celebrating the golden anniversary of the discovery of bacillosamine, the diamino sugar of a bacillus. Glycobiology **17**:1150–1155.
50. **Wyle FA, Artenstein MS, Brandt BL, Tramont EC, Kasper DL, Altieri PL, Berman SL, Lowenthal JP.** 1972. Immunologic response of man to group B meningococcal polysaccharide vaccines. J. Infect. Dis. **126**:514–521.
51. **Finne J, Leinonen M, Makela PH.** 1983. Antigenic similarities between brain components and bacteria causing meningitis. Implications for vaccine development and pathogenesis. Lancet **ii**:355–357.
52. **Skurnik D, Davis MR, Jr, Benedetti D, Moravec KL, Cywes-Bentley C, Roux D, Traficante DC, Walsh RL, Maira-Litran T, Cassidy SK, Hermos CR, Martin TR, Thakkallapalli EL, Vargas SO, McAdam AJ, Lieberman TD, Kishony R, Lipuma JJ, Pier GB, Goldberg JB, Priebe GP.** 2012. Targeting pan-resistant bacteria with antibodies to a broadly conserved surface polysaccharide expressed during infection. J. Infect. Dis. **205**:1709–1718.
53. **Prendergast MM, Moran AP.** 2000. Lipopolysaccharides in the development of the Guillain-Barre syndrome and Miller Fisher syndrome forms of acute inflammatory peripheral neuropathies. J. Endotoxin Res. **6**:341–359.
54. **Yuki N, Hartung HP.** 2012. Guillain-Barre syndrome. N. Engl. J. Med. **366**:2294–2304.
55. **Moe GR, Tan S, Granoff DM.** 1999. Molecular mimetics of polysaccharide epitopes as vaccine candidates for prevention of Neisseria meningitidis serogroup B disease. FEMS Immunol. Med. Microbiol. **26**:209–226.
56. **Harvey HA, Swords WE, Apicella MA.** 2001. The mimicry of human glycolipids and glycosphingolipids by the lipooligosaccharides of pathogenic neisseria and haemophilus. J. Autoimmun. **16**:257–262.
57. **Jann B, Jann K.** 1990. Structure and biosynthesis of the capsular antigens of Escherichia coli. Curr. Top. Microbiol. Immunol. **150**:19–42.
58. **Orskov F, Orskov I, Jann B, Jann K.** 1977. Serology, chemistry, and genetics of O and K antigens of Escherichia coli. Bacteriol. Rev. **41**:667–710.